CFD SIMULATION OF SOLAR AIR HEATER USING OBTUSE L ROUGHNESS

Thesis

Submitted to the

G.B. Pant University of Agriculture & Technology,
Pantnagar-263145, Uttarakhand, India

By

Mr. RAHUL PANT
ID. No. 57092

IN PARTIAL FULFILLMENT OF THE REQUIREMENTS FOR THE DEGREE OF

Master of Technology
In
Mechanical Engineering
(Thermal Engineering)

September, 2022

ACKNOWLEDGEMENT

I am overwhelmed with joy to evince my profound sense of reverence and gratitude to ***Dr. Lokesh Varshney, Professor, Department of Mechanical Engineering, G.B.P.U.A.&T., Pantnagar, and Chairman of my Advisory Committee****, for helping me in improving the draft, providing liberal guidance at every stage of this work, and providing me sufficient time for discussion as and when required. Since beginning up till the completion of this work he has been kind enough to motivate and encourage me. I would also like to thank him for encouraging and helping to shape my interests and ideas.*

I would like to express my deepest sense of gratitude and respect to the esteemed ***members of my Advisory Committee, Dr. D. S. Murthy, Professor, and Dr. Prashant Verma, Assistant Professor, Department of Mechanical Engineering, G.B.P.U.A.& T., Pantnagar*** *for their valuable suggestions at every stage of the work.*

I am thankful to ***Dr. Alaknanda Ashok, Dean, College of Technology*** *and* ***Dr. Kiran P. Raverkar, Dean, Post Graduate Studies, G.B. Pant University of Agriculture & Technology, Pantnagar*** *for providing necessary facilities to carry out this study.*

My other teaching and non-teaching staffs, Department of mechanical engineering definitely deserve a special work of thanks always being there to support and encrouge me.

During my study in the campus, I had been greatly supported and helped by number of friends. I express my sincere thanks to ***Ankur Haldar, Rishab Sharma, Ashutosh Joshi, Dheeraj Mohan Gururani, Manoj Singh Bohra, Shubham Mallik, Amit Kumar Shah, Gaurav Prakash Joshi, Pankaj Kumar, Harshit Saxena, Dheeraj Singh Rana, Mayank Tiwari and all other friends*** *for their help and encouragement given to me during the entire period of course in the campus.*

Last but not least, words run short to express my heartfelt gratitude to my beloved parents, ***Mother Mrs. Geeta Pant, Father Mr. Dinesh Chandra Pant, my elder brother Sqn. Ldr. Rakesh Pandey, My brother Mr. Ravi Pandey and my other family members****, whose filial affection, environment, love, and blessings have been a beacon of light for the successful completion of this achievement.*

Above all, my humble and whole heartily prostration to the Almighty for his Blessings.

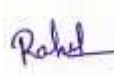

Place: Pantnagar ***(Rahul Pant)***

September, 2022 *Author*

CERTIFICATE – I

This is to certify that the thesis entitled **"CFD SIMULATION OF SOLAR AIR HEATER USING OBTUSE L ROUGHNESS"** submitted in partial fulfilment of the requirements for the degree of **Master of Technology** in **Mechanical Engineering** with major in **Thermal Engineering** of College of Post-Graduate Studies, G.B. Pant University of Agriculture & Technology, Pantnagar, is a record of bonafide research carried out by **Mr. Rahul Pant**, ID. No. **57092** under my supervision and no part of the thesis has been submitted for any other degree or diploma.

The assistance and help received during the course of this investigation have been acknowledged.

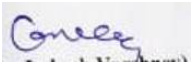

Pantnagar
September, 2022

(Lokesh Varshney)
Chairman
Advisory Committee

CERTIFICATE– II

We, the undersigned, members of the Advisory Committee of **Mr. Rahul Pant,** ID. No. **57092,** a candidate for the degree of **Master of Technology** in **Mechanical Engineering** with major in **Thermal Engineering** agree that the thesis entitled **"CFD SIMULATION OF SOLAR AIR HEATER USING OBTUSE L ROUGHNESS"** may be submitted in partial fulfilment of the requirements for the degree.

(Lokesh Varshney)
Chairman
Advisory Committee

(D. S. Murthy)
Member

(Prashant Verma)
Member

TABLE OF CONTENTS

LIST OF TABLES

LIST OF FIGURES

LIST OF ABBREVIATIONS

Abbreviation		Full Form
$\dot{m}$	:	Total mass flow of air entering and leaving the collector in kg/s
μ	:	Dynamic viscosity in Kg/m-s
A_c	:	Aperture area of the collector (L×w) in m^2
C_p	:	Specific heat at constant pressure of air in J/(kg °C)
D_h	:	Hydraulic diameter of the flow channel in m
e	:	Rib height
h	:	Convective heat transfer coefficient in w/(m^2 ^oC)
k	:	Thermal conductivity in W/m-k
Nu	:	Nusselt number
p	:	Pitch of roughness element
Re	:	Reynolds Number
THPP	:	Thermo-Hydraulic performance parameter
T_{in}	:	Inlet Temperature of Duct in ^oC
T_{mf}	:	Mean Fluid Temperature in ^oC
T_{mp}	:	Outlet Temperature of Duct in ^oC
T_{out}	:	Degree Centigrade
K	:	Kelvin
ρ	:	Density in Kg/m^3

Introduction

Chapter 1 INTRODUCTION

1.1 General

The greatest important resource and the best measure of a nation's success are considered to be per capita energy consumption. As the global population grows every day, so the demand for energy is also increasing. The backbone of the economy is regarded as energy. The biggest portion of a nation's Gross Domestic Product (GDP) originates in the energy industry.

On the basis of availability, the energy may be classified into two primary types:

I. Conventional source
II. Non-conventional source

1.1.1 Conventional sources

Conventional sources of energy are also known as non-renewable energy and these are available in limited quantity. Further, we can classify them as commercial and non-commercial. Coal, petroleum, and electricity are coming under commercial and firewood, straw comes under non-commercial conventional sources.

1.1.2 Non-conventional sources

Non-conventional sources of energy are also known as renewable energy and these are available in larger quantities. Examples can be solar energy, wind energy, geothermal energy, tidal energy, etc.

As we know that the conventional source of energy is limited, we have more consider the non-conventional source of energy to meet the demand of a large population and these types of conventional sources are also harmful to nature. So, scientists have to look for an alternate source of energy. If used appropriately, solar energy has a great deal of potential and the capacity to meet all energy demands.

Solar energy is a clean, dependable, and sustainable source of energy. The Sun's temperature is 5777 K. It is a sizable sphere of very hot gaseous stuff that is $1.5x10^{11}$ m from Earth and has a diameter of $1.39x10^{11}$ m. The Sun produces a total of around $3.8x10^{20}$ MW of energy, which is equal to $63x10^{6}$ W/m^2 of its surface. The core temperature is thought to be in the range of $8x10^{6}$ K to $40x10^{6}$ K. Out of the entire amount of radiation the Sun emits, only roughly 17×10^{13} kW gets transferred to the Earth. However, a year's worth of energy needs on Earth can be met with just thirty minutes of

this tiny portion of solar energy. For medium and low-temperature applications, the usesof this energy are quite practical. The need for energy resources is growing every day, and solar energy can assist meet that demand. Almost all of India receives 4 to 7 kWh/m^2 of solar radiation annually due to its location in the tropical zone, where temperatures are nearly always in the range of 25°C to 27°C. As a result, India has a good source for using solar energy.

1.2 Solar Collector

Incoming solar radiation is absorbed by this apparatus, which then transforms it into thermal energy at the absorbing surface and transfers it to a fluid passing through the collector. The flat plate collector and the concentrated collector are two different kinds of solar collectors. A solar collector known as concentrating solar collector directs sunlight onto a tiny area using reflective surfaces, where it is collected and transformed into heat or, in the application of solar photovoltaic equipment, converted to electricity. In contrast, a flat plate collector has an area of interception that is identical to that of absorption for solar radiations.

1.2.1 Flat Plate Collector

Flat plate collectors which are non-concentrating kinds of collectors are useful for temperature rise. Below 90°C are needed for applications like space heating and service water heating and other most practical purposes. They are constructed in rectangular panels that range in size from 1.7 to 2.9 m^2 and are easy to assemble. Both direct and diffuse radiation can be absorbed by flat plate collectors. **Fig. 1.1** depicts a flat plate collector. In which sunlight is coming to absorber plate. The absorber plate is covered with insulation box and two glass plates.

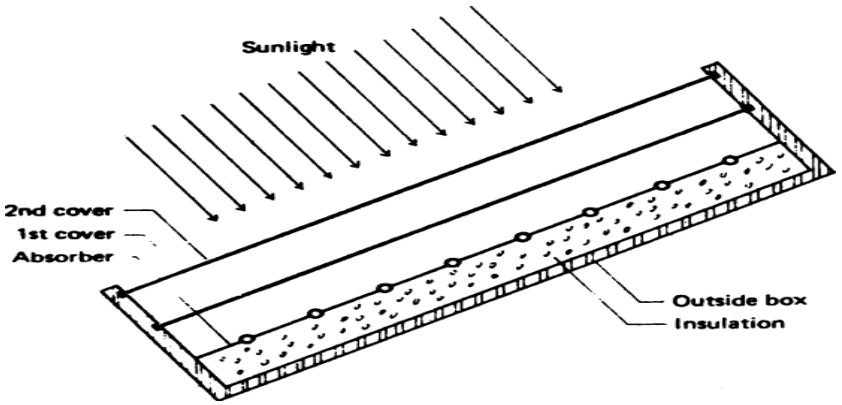

Fig. 1.1 Schematic of smooth flat plate collector (Sayigh, A.A.M., 1979)

Flat plate collectors can be categorized as solar liquid heaters and solar air heaters depending on the kind of working fluid they utilize.

1.2.2 Solar Liquid Heater

Solar water heaters heat water using the sun's natural light. **Fig. 1.2** presents a schematic diagram of solar air heater. It contains a flat surface known as the absorbing surface that absorbs solar energy efficiently. The most frequently used materials are typically metal plates, often made of copper, aluminum, and copper tubing in thermal interaction with the plate.

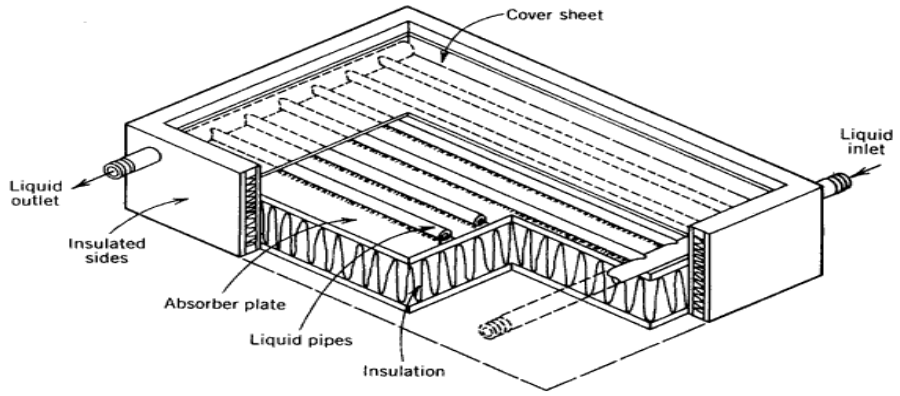

Fig. 1.2 Schematic of solar liquid heater (Rai, G.D., 2010)

1.2.3 Solar Air Heater

Due to the low cost and widespread usage, solar air heaters are the most popular and straightforward solar energy collection equipment. The primary uses of solar air heaters are for room heating, curing industrial products, seasoning wood, and drying out building materials made of concrete or clay **(Yadav and Bhagoria, 2013)**. A solar air heater has a straightforward construction and requires little upkeep. However, the efficiency is decreased because of the inadequate heat transmission between the absorber plate and air. This is why absorber surfaces are occasionally roughened **(Sukhatme and Nayak, 2011)**. In order to achieve the best possible arrangement of the roughness element, numerous studies using roughness elements of various shapes, sizes, and orientations with regard to flow direction have been conducted.

There are two kinds of solar air heaters: glazed and unglazed. To reduce heat losses, glazed solar air heaters have an insulated bottom and side surface in addition to transparent glass on the top sheet. Air flows above or below the absorber plate in glazed solar air heaters, removing heat from the absorber plate. It is employed for applications

like room heating and drying. While unglazed solar air heaters have a clear cover on the top sheet. In commercial buildings, it is applied for purposes such as preheating makeup air.

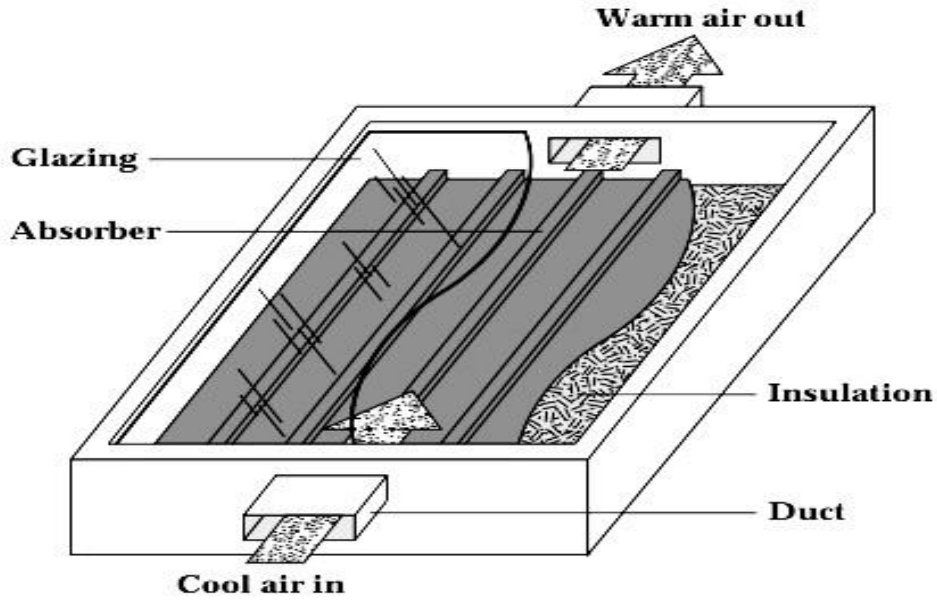

Fig. 1.3 Solar air heater (Rai, G.D., 2010)

Air may have certain benefits when used in solar collectors. These points are discussed below:

I. Because the air pressure at the entrance is atmospheric, the material used for the collector and duct in a solar air heater is light.

II. Because air is lighter than water, the working load on the collector is generally lower.

III. With the exception of some heat loss, a leakage in a solar air heater does not pose a severe threat.

a) Solar air heater with smooth absorber surface

There are no obstructions in the path of flowing air in solar air heaters with smooth absorber surfaces and laminar sub-layers forming in the heat transfer zone. As a result, the ability of the absorber plate to transmit heat to the air becomes minimal, which ultimately lowers thermal efficiency. The efficiency of solar air heater can be raised by some modifications-

I. Including fins to expand the area for heat transfer.

II. Raising the roughness of the plate's backside will increase turbulence and convective heat transfer coefficient.

b) Solar air heater with artificial roughened absorber surface

The heat transfer between the absorber plate of the solar air heater and air can be enhanced by either increasing the heat transfer surface area using extended surfaces or using artificial roughness on the absorber surface. Numerous techniques, including sandblasting, machining, casting, and shaping, welding ribs can be used to create roughness on the absorber surface. The most practical and cost-efficient technique to increase the solar air heater's efficacy is to apply artificial roughness in various shapes and sizes. In order to achieve the best possible positioning of roughness element geometry, several experimental investigations employing roughness elements of various shapes, sizes, and orientations with regard to flow direction have been conducted. The existence of a laminar/viscous sub-layer in addition to a turbulent core in a turbulent flow is widely established. The laminar boundary layer of turbulent flow is disrupted by the artificial roughness on the absorber surface, which causes the increment of heat transfer between air and absorber plate.

Joule (1861) was the first to use the notion of artificial roughness to improve heat transfer coefficients for steam condensation in tubes. Since then, numerous experimental investigations have been conducted on the use of artificial roughness in the cooling of gas turbines, electronic devices, nuclear reactors, etc.

There are some of the figures shows several different rib geometries. **Fig. 1.4** shows a wedge shape transfer rib roughness created on the absorber plate. It has three changing parameters like Rib height, rib pitch and wedge angle. **Fig. 1.5** shows arc shaped rib roughness created on absorber plate. This roughness created with the wire up to the length of 1000 mm. **Fig. 1.6** shows that W-shaped rib roughness which is created on the absorber plate.

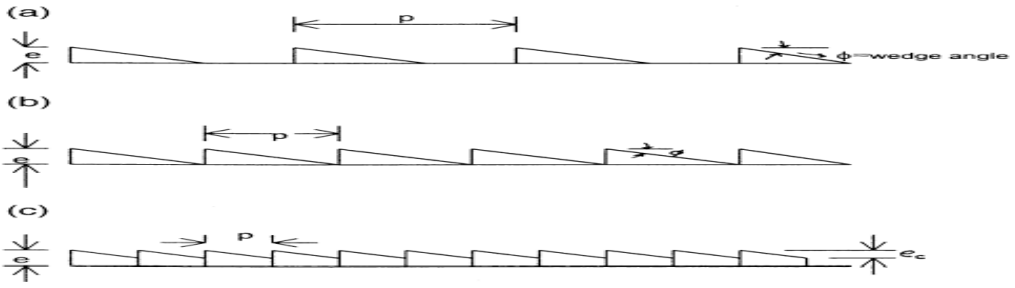

Fig. 1.4 Wedge-shaped transverse rib roughness (Bhagoria *et al.*, 2002)

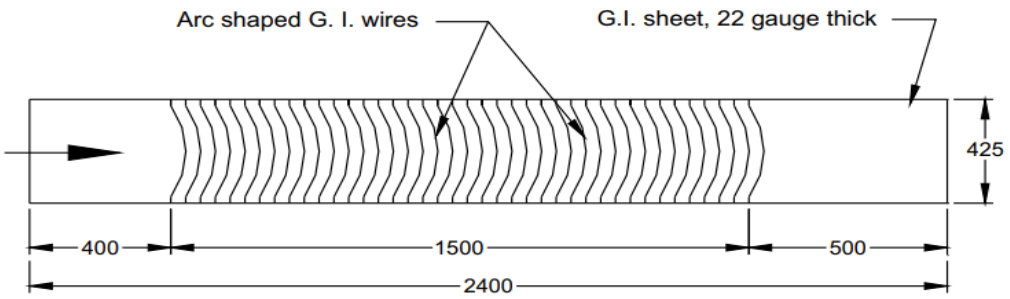

Fig. 1.5 Arc-shaped rib roughness (Saini and Saini, 2008)

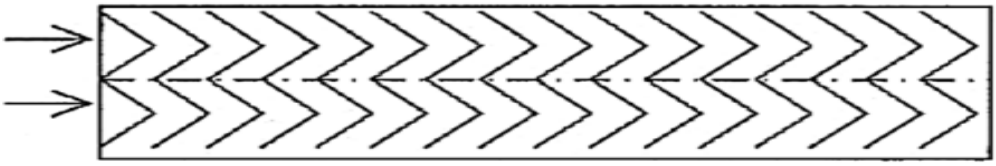

Fig. 1.6 W-shaped rib roughness (Lanjewar *et al.*, 2011)

1.3 Organization of Thesis

This is a description of each chapter of the thesis. The five chapters of the work are listed below.

Chapter 1 described the framework of the study, which highlights the many kinds of solar collectors along with other relevant concepts, connected to the topic. The goal of the study is to analyze how well artificial solar air heaters operate when the Reynolds number, roughness height, and roughness pitch are changed. This chapter also discusses the significance of the roughened solar air heater and the scope of our research.

Chapter 2 described a detailed literature review to find the goals of doing this research. It offers general literature on the idea of solar air heaters with smooth plates and solar air heaters with roughened absorber plates, having various types of geometry used by numerous investigators and their associated models. Finally, research was conducted to analyze the performance of solar air heaters with Obtuse L roughness on their absorber plates with the assistance of ANSYS Fluent 2022 R1.

Chapter 3 covered the materials and techniques used to analyze fluid flow from solar air heaters with smooth and roughened absorber plates. Additionally, in this chapter a variety of operational parameters including Reynolds number, roughness height, and roughness pitch are chosen for investigation. The study's context has included discussions

of the grid-independent test, solution methodology, and validation of the findings using the Dittus-Boelter for smooth plate solar air heater.

Chapter 4 described the results from the CFD analysis of the solar air heater with an Obtuse-L roughened absorber plate. The outcomes include the impact on Nusselt number and friction factor of several operational parameters including Reynolds number, relative roughness height, and relative roughness pitch. The thermo-hydraulic performance parameter is finally contrasted for the obtuse L roughness profile.

Chapter 5 summarized the data which highlights the benefit of the obtuse L roughness profile in solar air heater. The upcoming research directions are also covered in this chapter.

Closer

In this chapter, the importance of solar energy has been discussed. Additionally, different type of solar collector is discussed in this chapter. Various techniques to enhance the performance of solar collector have also been presented using different roughness geometries. Comparison of enhanced performance relative to smooth collector is also described.

Review of Literature

Chapter 2 REVIEW OF LITERATURE

2.1 General

We are well aware that the low amount of heat transfer coefficient contributes to the low efficiency of solar air heaters. To enhance the thermal efficiency of solar air heaters, numerous studies have been carried out recently. We can use one of three approaches to deal with the problem of fluid flow and heat transmission in solar air heater. These approaches are:

1. Theoretical
2. Experimental
3. Computational fluid dynamics (CFD)

2.2 Theoretical Approach-

Instead of being a true model, the mathematical model might be utilized to create a theoretical prediction. Differential equation sets are available for theoretical techniques. In order to monitor issues using a theoretical approach, several assumptions must be established.

Lewis (1975) showed the new approach that analyses the parameters that controlled the momentum transfer and heat transfer performance in a uniform channel flow. It is a novel efficiency parameter that is used to define the thermo-hydraulic performance of rough to smooth surfaces. The goal of this paper was to propose a method and design chart for analyzing and optimizing the thermo-hydraulic performance of rough surfaces in channels that use the equivalent hydraulic diameter concept.

Prasad and Saini (1988) researched the concert of wholly developed turbulent flow in the circular transverse wire rib roughness on to the absorber plate of solar air heater and expression for prediction of average Stanton number and average friction factor have developed. The Nusselt number had a mean deviation of 10.7 percent whereas the friction factor had a mean-variance of 6.3 percent. It has also been investigated how friction and heat transfer are impacted by roughness element height and pitch. It was discovered that as relative roughness height goes increases, the rate of heat transfer enhancement decreases, and the friction factor rises. On the other hand, as relative roughness pitch proceeds to increment, the rate of friction and heat transfer reduces.

Cortis and Piacetini (1990) constructed a steady state mathematical model for a roughened collector solar air heater, a steady state mathematical model was constructed. Friction and heat transfer into the rectangular ducts with periodic disturbances were used to assess the impact of such disturbances on bare collector efficiency and pressure drop. It shows that produced outcomes over the study Improvement of efficiency of a bare solar collector, incorporating wire-type periodic disturbances on absorber plate allows for efficiency improvements of 9 to 55 percent. Pitch reduction improves efficiency by a small amount. The addition of barriers, on the other hand, increases the amount of air power required. For low air-flow values (Re < 35000), the perturbation can improve the efficiency of the bare collector. The disturbances must be minor, and the pitch must increase as the airflow increases. If the Reynolds number is high within the limit, the existence of a disturbance must result in a minimum radiation intensity ($H > 600W/m^2$) for the performance to be improved.

Gupta *et al.* (1997) researched the effect of roughness on the thermal and hydraulic performance of roughened plate solar air heaters and compared with it to smooth solar air heaters. It has been determined what the best design and operation conditions are. Based on thermo-hydraulic considerations, it has been discovered that depending on the insolation, systems operating in a specific scale of Reynolds numbers have improved thermo-hydraulic performance. It discovered that for Reynolds values more than 10,000, the effective efficiency proceeds to increase as the insolation increases. The thermo-hydraulic efficiency declines with increased insolation at lower Reynolds numbers (Re < 10,000). It also found that with the increasing relative roughness height, the numerical value of the maximum effective efficiency is to found to decrease. Additionally, found that smooth solar air heaters perform better thermo-hydraulically, whereas roughened solar air heaters are thermo-hydraulically advantageous for lower Reynolds numbers, although the thermal efficiency of a roughened solar air heater may be higher than the smooth heater beyond a certain Reynolds number limiting value. The limiting Reynolds number has been determined to be between 13,000 and 19,000. The real value is determined by relative roughness height and amount of insolation.

Mittal *et al.* (2007) showed a comparison of the effective efficiency of solar air heaters with various roughness element geometry on absorber plates. Within the analyzed system parameters, the effective efficiency was determined by employing the friction

factor and heat transfer correlations developed by the various investigators. It was discovered that roughened ducts with various sorts of roughness elements improved the effective efficiency of solar air heaters significantly. The higher the Reynolds number, the better the effective efficiency of the solar air heater with inclined ribs as the roughness element.

Layek *et al.* (2007) proposed a mathematical model for simulating the entropy generation of chamfered rib-groove roughened absorber panel in a solar air heater. Roughness parameters like relative roughness pitch, relative roughness height, relative groove position, chamfer angle, and Reynolds number have a combined effect on heat transfer as well as fluid friction. It was discovered that as relative roughness height rises, entropy generation reduces. The minimum increase in entropy generation is shown by the configuration of relative roughness pitch of 6, relative groove position of 4, and 18^{o} chamfer angle.

Gupta and Kaushik (2009) conducted the parametric analysis of metal mesh type artificial roughness in an absorber plate of a solar air heater and compared it with smooth duct Performance assessments were done using the terms Energy Augmentation Ratio, Effective Energy Augmentation Ratio, and Exergy Augmentation Ratio for the different values of Reynolds number and the roughness parameters of metal mesh roughness geometry in absorber plate of solar air heater duct. In order of EEAR, EAR, and EXAR, the augmentation ratios fall at a quicker rate with Re. It's also discovered that the augmentation ratio rises as duct depth and solar radiation intensity rise. For a bigger flow cross-section area of solar air heater duct, low Re range, and higher solar radiation intensity, the EXAR is greater than unity. For the low range of Re, EXAR increases with roughness height.

Singh *et al.* (2012) developed a mathematical model for forecasting the energetic efficiency of the solar air heater with a discrete V-down rib roughened absorber panel. The impact of Reynolds number and rib-roughness parameter on energetic efficiency was investigated. For Reynolds number ranges typically smaller than 18000, the exergy-based criterion suggests using a discrete V-down rib roughened solar air heater. A smooth flat-plate solar air heater may be acceptable for Reynolds numbers more than 18,000. Exergetic efficiency may be negative with increasing Reynolds numbers.

Karwa and Shrivastava (2013) carried out a mathematical model which is used to find the thermal performance of a V-down discrete rib roughness solar air heater. In the winter season of Western Rajasthan. The collector, which delivers heated air for space heating applications, is positioned at a 45^{o} slope facing south and runs in a closed loop mode with incoming air at a fixed temperature of 295 K from confined space. The ambient temperature was from 278 to 288 K. The thermal efficiency of roughened duct air heater is 6 to 26% higher than a smooth duct air heater, according to the findings.

2.3 Practical Approach

Actual measurement is frequently the most dependable source of data on a physical process. Full-scale equipment can be used in an experimental manner to forecast how identical duplicates of the equipment would work under real-world situations. Comprehensive tests are costly, difficult, and frequently impossible. As an alternative, small-scale models can be used. However, the generated data must be extrapolated to the full-scale model. Small-scale models do not usually accurately represent all aspects of full-size equipment. As a result, the test results are less meaningful. The advantages of a practical approach are actual measurements of results and the ability to account for manufacturing errors in the results. Time-consuming and expensive setups are disadvantages; nonetheless, when a real prototype is available, a minimum of 3 to 5 prototypes must be evaluated. It is important to remember that many conditions are challenging to measure and that measuring tools are not free of faults (Patankar 1980).

The testing methodologies for the thermal performance of solar collectors were detailed in a variety of standards. The ASHRAE Standard 93-77 is the most well-known. It generally uses to assess the efficiency of flat plate and concentrator solar collectors. For the purpose of the test measuring the following parameters is required:

a) Global solar irradiation at the collector plate
b) Diffuse solar irradiance at the collector aperture
c) Airspeed above the collector aperture
d) Ambient air temperature
e) Fluid temperature at collector inlet
f) Fluid temperature at collector outlet
g) Fluid flow rate

Because solar radiation is absorbed by the absorber plate, which is the primary heat transmission surface in a solar air heater, the solar air heater is modeled as a rectangular channel with one rough wall and three smooth walls. The next sub-sections go through the general arguments for several sorts of roughness geometries that have been explored experimentally by various investigators.

Varshney and Saini (1998) conducted experimental studies to determine the fluid flow properties of solar air heaters with a duct filled with wire mesh screen matrices. The investigations included a broad variety of wire mesh screen matrix geometrical characteristics like wire diameter, pitch, and a number of layers. For air moving through a bed of wire mesh screen matrix fill up in solar air heater duct in a cross-flow configuration, generalized correlations for friction factor and heat transfer coefficient have been derived.

Verma and Prasad (2000) carried out an outdoor experimental investigation for thermohydraulic optimization of the roughness and flow parameters for Transverse wire rib roughness of solar air heater. Reynolds number ranges from 5000 to 20000, relative roughness pitch ranges from 10 to 40 along with relative roughness height ranges from 0.01 to 0.03 are taken into consideration as input parameters. The author detailed how the roughness of the transverse wire affected the heat and fluid flow properties of three rectangular surface air heater ducts, two of which had roughened collectors and one that had a plane surface. According to research, the ideal roughness Reynolds number is 24, and the ideal thermal-hydraulic performance is 71 percent at this value. For the parameters examined, it was discovered that the heat transfer enhancement factor varied from 1.25 to 2.08.

Karwa *et al.* (2001) provide the findings of an experimental study of the performance of a solar air heater with a chamfered repeating rib-roughness on the absorber plate airflow side. With a 15° rib chamfer angle, the roughened portions had comparative roughness pitches of 4.58 and 7.09, respectively. For airflow duct depths of 16, 21.5, and 21.8 mm with Reynolds numbers ranging from 3750 to 16350 whereas relative roughness heights for the three roughened plates used are 0.0441, 0.0256, and 0.0441, respectively. Due to the increment in Nusselt number, the study demonstrates a significant increase in thermal efficiency varies from 10 % to 40% over solar air heaters using smooth absorber

panels varies from 50 % to 120 %. Due to the rise in the friction factor, the increased thermal efficiency is followed by a significant increase in the pumping power needed from 80 % to 290 %. The solar air heater with roughness components with a high relative roughness height performs better at low flow rates, corresponding to the applications needing air at a high temperature. The relative gain in energy collection with increasing relative roughness height, however, is greater at high flow rates than the increase in pumping power. The net advantage is therefore greater at lower roughness heights. At greater flow rates, the smooth duct air heater offers better effective efficiency.

Karwa *et al*. (2001) investigated experimentally the outcome of the geometrical parameter of the V-shaped ribs on heat transfer and fluid flow characteristics of the rectangular duct of a solar air heater with an absorber plate with V-shaped ribs on its bottom. The experiment covered a Reynolds number range of 2500 to 18000, a relative roughness height range of 0.02 to 0.034, and a flow angle of attack range of 30^o to 90^o with a fixed relative pitch of 10. The outcomes were compared to those of a smooth duct under comparable flow conditions in order to gauge the improvement in friction factor. The following are some of the inferences that can be like with an increase in Reynolds number, the Nusselt number rises while the friction factor falls. This is owing to a distinct change in fluid flow characteristics caused by roughness, which generates flow separations, reattachments, and secondary flow generation. For an angle of attack of 60 degrees, the highest increase in Nusselt number and friction factor as a result of artificial roughness was determined to be 2.30 and 2.83 times that of the smooth duct. It was discovered that the maximum values for both the Nusselt number and friction factor correlate to the same angle of attack. The thermo-hydraulic performance improves as the relative roughness height and angle of attack of flow increase, with a maximum of 60^o.

Bhagoria *et al. (*2002) studied airflow in a rectangular duct with one roughened wall exposed to uniform heat flux and the other three smooth walls insulated. The flow in the duct of the solar air heater corresponds to these characteristics. The Reynolds number ranged from 3000 to 18000, with relative roughness heights ranging from 0.015 to 0.033 and rib wedge angles of 8, 10, 12, and 15^o in the experiment. The influence of various parameters on a heat transfer coefficient and a friction factor is compared to the outcome of a smooth duct with similar flow conditions. The main conclusions are as follows: For the set of parameters examined, the existence of ribs increases the Nusselt number by 2.4

times and the friction factor by 5.3 times when compared to the smooth duct. When the relative roughness pitch is around 7.57, as the relative roughness pitch increases, the heat transfer is at its highest, yet the friction factor is decreasing. While the Nusselt number drops on either side of the wedge angle, the greatest increase in heat transfer occurs at a wedge angle of around 10°. The friction factor rises as the wedge angle does as well.

Mittle and Varshney (2006) were concerned with conducting thermo-hydraulic analyses on a solar air heater with a packed bed that has a conduit filled with blackened wire screen matrices with various geometrical properties (wire diameter and pitch). By deducting the primary energy required to produce the power required to pump air through the packed bed from the actual thermal energy gain, the thermo-hydraulic performance of solar air heaters are measured in terms of effective efficiency. A mathematical model is created to calculate effective efficiency based on the energy transfer mechanism in the bed. The numerous discoveries include the fact that wire mesh-packed solar air heaters are more effective than traditional smooth air heaters. It also discovered that the effective efficiency values closely match the thermal efficiency values for larger values of the temperature rise parameter, however, there is a noticeable discrepancy for lower values of the temperature rise parameter.

Sahu and Bhagoria (2005) carried out an experimental investigation to assess the heat transfer coefficient using 90^{o} broken transverse ribs on the absorber plate of the solar air heater. The roughened wall was heated while the remaining three walls were insulated. The roughened wall features roughness with a pitch of 10–30 mm, a rib height of 1.5 mm, and an aspect ratio of 8 for the duct. The airflow rate is related to the Reynolds number, which ranges from 3000 to 12,000. To estimate the thermal efficiency of solar air heaters, the heat transfer results were compared to the smooth ducts with similar flow and thermal boundary conditions. The following results have been taken from this investigation: the Nusselt number grows across the Reynolds number range, reaches a maximum for roughness pitch of 20 mm, and then declines as roughness pitch increases. At low Reynolds numbers, the Nusselt number grows fast, then becomes constant or slightly increases in contrast to low Reynolds numbers. This also met our goal of using a solar collector with a low Reynolds number. The highest increase in heat transfer coefficient occurs at a pitch of roughly 20 mm, whereas the Nusselt number drops on either side of

this pitch. It was also discovered that a smooth duct performs better than an artificially roughened duct at low Reynolds numbers (below 5000).

Jaurker *et al*. (2006) investigated experimentally the friction characteristics and heat transfer of the rib-grooved artificial roughness on one heated wall of a large aspect ratio duct and it was discovered that the Nusselt number can be increased beyond that of the ribbed duct while taking the friction factor enhancement low. The Reynolds number varied from 3000 to 21,000, the relative roughness height was 0.0181 to 0.0363, the relative roughness pitch was 4.5 to 10, and the groove position to pitch ratio was 0.3 to 0.7. The following are the main conclusions that have been taken in the range of parameters studied, the presence of rib grooved artificial roughness increases the Nusselt number up to 2.7 times and the friction factor up to 3.6 times when compared to a smooth duct. For a relative roughness pitch of roughly 6.0, the maximum heat transmission occurs, and it decreases on both sides of the relative roughness pitch, with a similar trend for friction factor. The rib-grooved arrangement is proven to have the best thermo-hydraulic performance and can thus be used for heat transfer enhancement.

Layek *et al*. (2007) quantitatively investigated the creation of entropy in a solar air heater duct with repeated transverse chamfered rib–grooved roughness on one of the large walls. Fluid friction and heat transfer are affected by roughness characteristics such as relative roughness pitch, relative roughness height, relative groove location, chamfer angle, and flow Reynolds number. The effect of the roughness parameter on the creation of entropy is investigated. It was discovered that as relative roughness height increases, the entropy generation reduces. The entropy generation is lowest when the relative roughness pitch is 6, the relative groove position is 0.4, and the chamfer angle is 18^{o}.

Varun *et al*. (2008) used a combination of transverse and inclined ribs on the absorber plate of a solar air heater, an experimental inquiry was carried out to evaluate the heat transmission and friction characteristics. The Reynolds number ranged from 2000 to 14000, the relative roughness pitch was 3–8, and the relative roughness height was 0.030 in an experimental study. In this study, the effect of these factors on the friction factor and friction factor is explored, and Nusselt number and friction factor correlations are created within practical ranges. It is found that the geometry with the highest thermal efficiency is the one with a relative roughness pitch of 8. The thermal performance of a roughened solar

air heater has been determined analytically. It is observed that the proposed approach can be used to accurately anticipate the performance of solar air heaters.

Saini and Saini (2008) conducted an experimental study to improve the heat transfer coefficient of solar air heater with roughened air duct and an artificial roughness element in the form of an arc shape parallel wire with Reynolds numbers ranging from 2000 to 17000. It has been determined that giving arc-shape parallel wire geometry as artificial roughness with solar air duct results in an increase in heat transfer coefficient. The largest Nusselt number enhancement was 3.80 times, which corresponds to a relative arc angle of 0.3333 at a relative roughness height of 0.0422. The increase in friction factor corresponding to these parameters, on the other hand, has only been recorded 1.75 times.

Saini and Verma (2008) investigated experimental research of roughness and operating parameters on heat transfer and friction factor in a roughened duct with dimple-shape roughness geometry. The Reynolds number ranged from 2000 to 12,000, the relative roughness height from 0.018 to 0.037, and the relative pitch from 8 to 12. The optimum value of the Nusselt number was discovered to correspond to a relative roughness height of 0.0379 and a relative pitch of 10. The friction factor's minimal value corresponds to a relative roughness height of 0.0289 and a relative pitch of 10. As a result, the geometry's roughness characteristics can be chosen based on the net heat gain and corresponding power required to move air through the duct.

Aharwal *et al*. (2009) present an experimental study of heat transfer and friction properties of solar air heater duct with integral repeating discrete heat transfer. The absorber plate has square ribs. The impact of geometrical features, particularly gap width and gap position, has been studied. The width-to-height ratio of the roughened duct is 5.83. The kinship the relative gap position and relative gap width have varied from 0.16 to 0.5 and 0.5–2.0, respectively. Experiments were conducted for Reynolds numbers ranging from 3000 to 18,000, with relative roughness pitch ranging from 4 to 10, relative roughness height ranging from 0.018 to 0.037, and angle of attack ranging from 30^{o} to 90^{o}. This research leads to the following conclusion: For the range of parameters studied, the rib-roughened surface gives an increase in the friction factor and Nusselt number of roughly 2.83 and 3.60 times, respectively, when compared to the smooth surface. For the relative roughness pitch of 8.0, angle of attack of 60^{o}, and relative roughness height of

0.037, the highest heat transfer enhancement occurs at the relative gap position of 0.25 with the relative gap width of 1.0. For discrete transverse ribs with a relative roughness pitch of 8.0, the friction factor reaches its maximum value.

Karmare and Tikekar (2009) provide the findings of an experimental study of roughened solar air heater with metal rib grits thermo hydraulic performance. This research leads to the following conclusion: At low Reynolds numbers, the rate of growth of usable energy gain is substantially larger, but it is slightly lower at higher Reynolds numbers. However, the rate of increase in power consumption is modest in the lower Reynolds number range and grows at a reasonably fast rate as the Reynolds number rises. For a given roughness configuration, there is an optimum operating condition where the effective efficiency is highest for a given Reynolds number. The maximum value of effective efficiency shifts to a higher Reynolds number as the value of insolation rises. As a result, the flow should be adjusted to a Reynolds number in order to ensure the highest effective efficiency for that value of insolation. As the wedge angle increases, the friction factor rises.

Kumar *et al*. (2009) carried out an experimental investigation to study the friction characteristics and friction characteristics in solar air heaters Using discrete W-shape roughness on one wall of a solar air heater with an aspect ratio of 8:1. The roughened wall was heated while the remaining three walls were insulated. The Reynolds number ranged from 3000 to 15,000, the relative roughness height was 0.0168 to 0.0338, the relative roughness pitch was 10, and the angle of attack was 30^{o} to 75^{o}. It was discovered that the rate of increase of Nusselt number with an increase in Reynolds number is lower than the rate of increase of friction factor. For an angle of attack of 60 degrees, the highest increase in Nusselt number and friction factor as a result of artificial roughness was determined to be 2.16 and 2.75 times that of the smooth duct. It was discovered that the maximum values of both the Nusselt number and the friction factor correlate to the same angle of attack. It appeared that flow separation and secondary flow caused by discrete W-shaped ribs, as well as the movement of the associated vortices, combine to produce an optimal angle of attack.

Bopche and Tandale (2009) carried out an experiment to examine the friction factor and friction factor of Artificial roughness in the form of specifically constructed inverted

U-shaped turbulators on the absorber surface of a solar air heater. The roughened wall is heated uniformly, while the other three walls are insulated. The Reynolds number ranged from 3800 to 18000 in the experiment. The following results have been drawn Roughness pitch has a significant impact on the flow pattern and, as a result, the duct's performance increases. Even at a low Reynolds number like less than 5000, when ribs are inefficient, the turbulator geometry demonstrates a significant heat transfer increase. The highest increase in Nusselt number and friction factor for Reynolds number 3800 is on the order of 2.388 and 2.50, respectively. The maximum Nusselt number and friction factor enhancements over smooth duct at a pitch of roughly 10 mm and turbulator tip height of 1.5 mm are on the order of 2.82 and 3.72, respectively. Turbulences generated only in the viscous sub-layer region of the boundary layer result in improved thermo-hydraulic performance, i.e., maximum heat transfer enhancement with minimal friction penalty.

Kumar *et al*. (2009) provides the findings of an experimental study of heat transfer and friction in airflow in a rectangular duct with several V-shaped ribs and gap roughness on one broad wall. Relative gap distance values of 0.24 to 0.80, relative gap width values of 0.5 to 1.5, relative roughness height values of 0.022 to 0.043, related roughness pitch values of 6 to 12, relative roughness width ratio values of 1 to 10, angle of attack range of 30 to 75 were all investigated. The following are the main conclusions the presence of a multi-V-shaped rib with gap artificial roughness increases the Nusselt number up to 6.74 times and the friction factor up to 6.37 times when compared to a smooth duct. For multi-V-shaped with gap rib, the Nusselt number and friction factor are higher than for continuous multi-V-shaped rib. For multi-V-shaped with gap rib and relative roughness width of 10, the friction factor reaches its maximum value.

Hans *et al*. (2010) performed an experimental investigation into the effect of multiple v-rib roughnesses on heat transfer coefficient and friction factor in a solar air heater duct that has been intentionally roughened. The Reynolds number was varied from 2000 to 20000, relative roughness height values were varied from 0.019 to 0.043, relative roughness pitch was varied from 6 to 12, angle of attack was varied from 30^{o} to 75^{o}, and relative roughness breadth was varied from 1 to 10. For the number of parameters investigated, the greatest increase in friction factor and Nusselt number due to the existence of such an artificial roughness was found to be 6 and 5 times, respectively, in contrast to the smooth duct. Maximum heat transfer enhancement is obtained at a relative

roughness width of 6, whereas the maximum friction factor is found at a relative roughness width of 10. It was also discovered that the Nusselt number and friction factor reach their maximum values at an angle of attack of 60^{o}. The maximum increase in Nusselt number and friction factor was recorded when relative roughness pitch was set to 8, and Nusselt number and friction factor increased monotonically as relative roughness height increased.

Lanjewar *et al.* (2011) investigated experimentally the thermo-hydraulic performance of a solar air heater with W-shaped ribs on the absorber plate, with the roughened wall being heated and the remaining three walls being insulated. The flow has been tested with W-shaped ribs pointing both downstream (W-down) and upstream (W-up). The airflow rate is proportional to the Reynolds number, which ranges from 2300 to 14000. W-down ribs have a maximum thermo-hydraulic ratio of 1.95, whereas W-up ribs have a maximum of 1.73. The w-down rib arrangement provides superior heat transmission performance than W-up rib arrangement based on thermo-hydraulic performance.

Singh *et al.* (2012) proposed a mathematical model for forecasting the exergetic efficiency of a discrete V-down rib roughened absorber plate solar air heater. Reynolds number and rib-roughness factors effects on exergetic efficiency are investigated. For Reynolds number range commonly employed in solar air heaters, i.e. for Reynolds numbers less than 18,000, the exergy-based criterion supports using the discrete V-down rib roughened solar air heater. The flat plate solar air heater is appropriate for Reynolds numbers greater than 18,000. The exergetic efficiency may be negative at higher Reynolds numbers when the exergy of pump work required surpasses the exergy of heat energy received by the solar air heater.

Sethi *et al.* (2012) investigated experimentally the influence of artificial roughness on heat transfer and friction characteristics in a solar air heater duct with dimple-shaped components organized in angular fashion (arc) as roughness elements on the absorber plate for a variety of system and operational parameters. The aspect ratio of the duct is 11, the relative roughness pitch is 10 to 20, the relative roughness height is 0.021 to 0.036, the arc angle is 45^{o} to 75^{o} and the Reynolds number is 3600 to 18000. It has been determined that the Nusselt number rises while the friction factor falls as the Reynolds number rises.

When compared to smooth surfaces, the friction factor and Nusselt number are larger. The greatest Nusselt number was discovered to correspond to 0.036 relative roughness height, 10 relative roughness pitch, and 60^{o} arc angle.

Ravi and Saini (2016) investigated experimental research on the effect of roughness on the Thermo hydraulic performance of double pass duct with discrete multi-V-shaped. The Reynolds number (Re) values used in the investigation ranged from 2000 to 20000. According to the findings, the heat transfer rate through the solar air heater double pass channel has been found to be greatly boosted. However, when compared to a single pass flow, the increase in pressure loss is equally large. The Nusselt number and friction factor are found to be major determinants of roughness characteristics. The Maximum Nusselt number ratio and friction factor ratio were found to be 3.4 and 2.5, respectively.

Gabhane and Patil (2017) conducted an experiment on thermal and hydraulic performance of a Double pass flow Solar Air Heater roughened with numerous C-shape ribs. For varied rib geometries with diverse pitch distance, angle of attack, Reynolds number and three rib angles were used. The following conclusion was reached like double flow over a single flow setup, the Solar Air Heater performs better. The use of multiple C-shape arrangements on both sides of the absorber allows for higher heat transfer than scattered C-shape roughness. The experiment uses three roughness angles and five pitch distances. In other words, fifteen roughness models were investigated. For a relative roughness pitch of 24, a roughness angle of 90^{o}C, and a Reynolds number of 15000, maximum Nusselt number were 415. The Nusselt number, friction factor, Stanton number, and thermo hydraulic performance parameter all have statistical correlations that offer maximum average variances of less than 12% with reasonable precision.

Komolafe *et al*. (2019) presented experimental research and thermal analysis of rectangular roughness on the absorber plate of the solar air heater. The solar air heater that was utilized in the experiment was made locally. During the daytime hours of 9:00–18:00 h operation, the highest solar radiation intensity, ambient, and solar air heater temperatures were 827.87 W/m2, 33.77^{o}C, and 112 °C respectively. The solar air heater's simulated maximum and minimum temperatures were 127^{o}C and 21 ^{o}C, respectively with the experimental results of 112^{o}C and 20^{o}C.

2.4 Computational Fluid Dynamics (CFD) Approach

Computational fluid dynamics (CFD) is the science of prognosticating fluid flow, heat and mass transfer, chemical reactions, and related phenomena. To prognosticate these phenomena, CFD solves the NAVIER-STROKE equation for the conservation of mass, momentum, and energy.

CFD is used in all stages of the engineering process:

a) Conceptual studies of new design
b) Detailed product development
c) Optimization troubleshooting
d) Redesign

CFD analysis complements testing and experimentation by reducing the total effort and cost required for experimentation and data acquisition.

Chaube *et al.* (2006) performed a computational study of heat transfer due to roughness in the form of ribs, heated wall of the rectangular duct for turbulent flow. Using commercially available CFD software, FLUENT 6.1, a 2D analysis of heat transfer and fluid flow through a rectangular duct of an artificially roughened solar air heater was performed. CFD analysis was performed on an artificially roughened solar air heater with ten different rib shapes, including rectangular, square, chamfered and triangular and so on. The SST K-ω turbulence model for shear stress transport was chosen by comparing the predictions of other turbulence models with experimental data. The range of Reynolds numbers is 3000 to 20000, which is essential in solar air heaters. The following findings are derived based on the current analysis like when compared to 3D models; the 2D analytical model produces results that are closer to those obtained experimentally. In comparison to 2D models, 3D models take significantly more memory and computing effort. As a result, it is sufficient to use a simplified 2D model that requires less memory and processing time. Chamfered ribs provide the best heat transfer, although rectangular ribs of size 3*5 mm provide the optimum performance index. The reattachment sites are where local heat transfer peaks. In the inter-rib regions, the turbulence intensity is highest at the crest of the local heat transfer coefficient.

Kumar and Saini (2009) investigated the performance of solar air heater ducts with artificial roughness in form of thin circular wire in arc-shaped geometry using Computational Fluid Dynamics. Three-dimensional models were used to analyze the heat transmission and flow of the chosen roughness element. On the absorber plate, ribs were added, while the opposite side of the duct was left smooth. The commercial CFD code FLUENT 6.3.26 was used for simulation. The range of Reynolds numbers is 6000 to 18000 and solar radiation of 1000 W/m^2 has been taken. For the analysis, various turbulence models were used, and the results were compared. The results of the k- ε model based on renormalization-group (RNG) have been found to be in good agreement, and this model is now utilized to predict heat transfer and friction factors in the duct. For an overall enhancement ratio of 1.7 was observed corresponding to a relative arc angle of 0.333 and a relative roughness height of 0.0426.

Karmare and Tikekar (2010) investigated the heat transmission and fluid flow in a rectangular duct with metal grit ribs used as roughness components on one broad wall of a solar air heater using Computational Fluid Dynamics (CFD). Commercial CFD code FLUENT 6.2.16 was used as a solver. Standard k- ε turbulence model was used to simulate. The same Reynolds number was tested on circular, triangular, and square rib grits with angles of attack of 54^o, 56^o, 58^o, $60^{o,}$ and 62^o. Consistent heat flux is applied to the broad wall. The Reynolds number range of 3600 to 17000 is maintained. The author found that the rate of heat transmission from the absorber plate to the flowing air is improved by artificial roughness on the underside of the absorber plate of the solar air heater. Among the many shapes and orientations investigated, the absorber plate with a square cross-section rib with a 58^o angle of attack produces the best results. The heat transmission efficiency of the 58^o rib inclination plate is found to be around 30% higher than that of the smooth plate. As a result, this sort of surface roughness plate is recommended for usage in solar air heaters.

Yadav and Bhagoria (2013) carried out a computational fluid dynamics analysis to pick the optimal turbulence model for the design of a solar air heater. Fluid flow through a traditional solar air heater is simulated using the current CFD code ANSYS FLUENT v12.1. It is assumed that the flow is two-dimensional. The effects of five different turbulence models on the quality of the obtained results are investigated: Standard k– ε turbulence model, Realizable k– ε turbulence model, Renormalization-Group (RNG) k– ε

turbulence model, Standard k– ω turbulence model, and Shear Stress Transport (SST) k–ω turbulence model. The Renormalization-Group k– ε model appears to produce the best results for two-dimensional flows through a standard solar air heater, according to the calculations.

Yadav and Bhagoria (2014) investigated heat transfer of fully developed turbulent flow in a rectangular duct with repeated transverse square sectioned rib roughness on the absorber plate. To model turbulent airflow through an intentionally roughened solar air heater, the commercial finite-volume CFD code ANSYS FLUENT version 12.1 is employed. The Navier-Stokes equations and the energy equation are solved using the RNG k- ε turbulence model with a low Reynolds number. Twelve different square sectioned rib configurations (relative roughness pitch: 7.14 to 35.71 and relative roughness height: 0.021 to 0.042) were examined. The duct's flow Reynolds number ranged from 3800 to 18,000, making it ideal for solar air heaters. The following are some of the study's key findings. For a relative roughness pitch of 7.14 and a relative roughness height of 0.042, the highest enhancement of the average Nusselt number was determined to be 2.86 times that of the smooth duct. At a Reynolds number of 15000, the average Nusselt number increases to its maximum. The value of the thermo-hydraulic performance parameter varies between 1.22 and 1.88.

Premanik *et al.* (2017) investigated the Computational Fluid Dynamics simulation of heat transmission and friction characteristics in a rectangular duct of a solar air heater with isosceles right triangle rib shape on the absorber plate. The roughness has been positioned so that the hypotenuse is facing the flow direction. Reynolds number, roughness height, and roughness pitch were chosen as the study's design parameters. Renormalization group (RNG) k- ε is the turbulence model used in CFD solutions. At roughness pitches of 5mm, 10mm, 15mm, and 20mm, roughness heights of 0.5mm, 1.0mm, and 1.5mm are chosen. For a relative roughness pitch of 5 and a relative roughness height of 0.03, the best thermo-hydraulic performance is obtained. In comparison to a smooth plate, the maximum increase in friction factor was 3.45 times.

Mahanand and Senapati (2020) investigated heat transfers and flow fields in solar air heater ducts with transverse inverted-T-shaped ribs. Considering a fixed value of relative roughness height of 0.042, the relative roughness pitch and Reynolds number are

varied from 7.14 to 17.86 and 3800 to 18,000, respectively. The study uses a two-dimensional computational domain in which an aluminum absorber plate is subjected to a constant and uniform heat flux of 1000 W/m^2. The RNG k- ε model with increased wall treatment is the most widely acknowledged turbulence model. At Reynolds, number 15,000, the greatest Nusselt number enhancement ratio with relative roughness pitch of 7.14, and maximum Nusselt number are roughly 2.747 times of the smooth duct. At Reynolds number 15,000, Thermal Enhancement Factor was 1.86 for a relative roughness pitch of 7.14 and a relative roughness height of 0.042.

Kumar *et al.* (2021) conducted numerical research in order to improve the thermal performance of the Solar Air Heater using an artificial rough absorber plate. The forward and backward trapezoidal rough ribs, as well as a polygonal transfer rib, were chosen for simulation study using ANSYS Fluent version 13.0. To anticipate the augmentation, the Renormalization k- ε model was chosen. The analysis looked at the performance of the proposed rib's Nusselt number and friction factor at Reynolds numbers ranging from 3800 to 18000. The results show that a polygonal rib shape with a relative roughness pitch of 3.33 produces a higher Nusselt number and a steady decrease in the Reynolds number 18000 friction factor. In the backward trapezoidal rib, the thermal-hydraulic performance parameter reached a maximum of 1.89 in a relative roughness pitch of 10 & relative roughness height of 0.06 at a Reynolds number of 15000.

Haldar *et al*. (2022) investigated computational fluid dynamics simulation of solar air heater with generated wave roughness using ANSYS FLUENT software. Twelve type of wavy surfaces with rib heights of 0.7 mm, 1 mm, and 1.4 mm and pitch of 10mm, 15mm, 20mm, and 25 mm were investigated for roughness elements. The related differential equations were solved using a finite volume approach on a 2D computational domain. The RNG k- ε turbulence model with increased wall function is being used to solve the transport equations for turbulent flow and energy dissipation rate, for a 1000 W/m^2 uniform heat flow. The THPP maxima for all geometries (pitch and rib height) are usually around the Re value of 12000 for all geometries. The highest THPP value is found for geometry with a relative roughness pitch of 21.43, a relative roughness height of 0.021, and a Re of 12000. The greatest THPP value is found to be 1.96.

Kalpana *et al.* (2022) performed a theoretical and practical study to evaluate the efficiency of heat transmission and pressure drop in a double-pass solar air heater with arc-shaped roughness. Investigations are conducted for Reynolds numbers between 3000 and 12,000, relative roughness pitches between 8 and 12, relative roughness heights between 0.043 and 0.0433, and an angle of attack 0.3333. Different performance metrics, including Nusselt number, friction factor, and thermal performance parameter have been examined. For Reynolds number of 11,283 and relative roughness pitch of 8 and relative roughness height of 0.0433, the increment in the Nusselt number for the rough double-pass solar air heater is achieved as 1.7 times that of the smooth double-pass solar air heater. For this thermal performance factor produced as 1.4.

After reading the literature study, it appears that L-profile and Inverted-T profiles produce excellent results, however there is a concern with heat accumulation that can be solved by giving an angle to the L shape. This modification may result less heat accumulation, reduce the pressure drop and better heat transfer. For that thermohydraulic performance parameter (THPP) can increase.

2.5 Objectives of Present Work.

In light of the foregoing, the investigation uses ANSYS to analyze the features of fluid flow along with heat transfer with the following specific goals like performance analysis of solar air heater with intentionally roughened surface based on CFD. Also examine the effectiveness of a solar air heater that has been intentionally roughened by adjusting the Reynolds number, flow direction, and roughness pitch and recommending ideal parameters for designers.

Closer

In this chapter, work done by the previous investigator has been thoroughly discussed. On the basis of literature survey, literature gap was observed which forms the basis of present study. And at last objective of present work has been mentioned.

Materials and Methods

Chapter 3 MATERIALS AND METHODS

3.1 General

The convective heat transfer coefficient and friction factor must be examined in order to analyze the impact of artificially created obtuse- L roughness on the collector plate of the Solar air heater. From this, we can find out the hydraulic effectiveness of the solar air heater. Generally, our motive is to increase heat transfer between collector plate to fluid medium and reduces the pressure drop and this helps to get optimum hydraulic effectiveness of the solar air heater.

This study attempted to examine the aforementioned parameters on various geometries using computational fluid dynamics (CFD). To more thoroughly analyze of temperature and flow conditions, the finite volume method is used. The CFD simulations were performed using ANSYS FLUENT software, which is available for purchase. Numerous physical laws and transport equations are used to solve the physics of the condition because CFD is the most accepted tool for the analysis of many different problems. These solutions are then further validated using previously published work and accepted empirical relations to ensure the model's accuracy. The outcomes are discovered to be in strong accord with the earlier papers reported. The following sections provide further details on the analysis's methodology.

3.2 Computational fluid dynamics (CFD) Methodology

The naiver-Stokes equation is the basis of all computational fluid dynamics (CFD) problems. The enormous potential of CFD made it very helpful in analyzing and researching. It also has a larger impact by reducing costs and time with respect to experimental investigations, which need more resources, time, money, and effort to test under the same settings. CFD has made significant progress in the study of solar air heaters during the past few decades. The phases are detailed in the CFD technique flow chart, which is seen in **Fig. 3.1**. The computational domain has three zones:

I. Inlet section
II. Test section
III. Outlet section

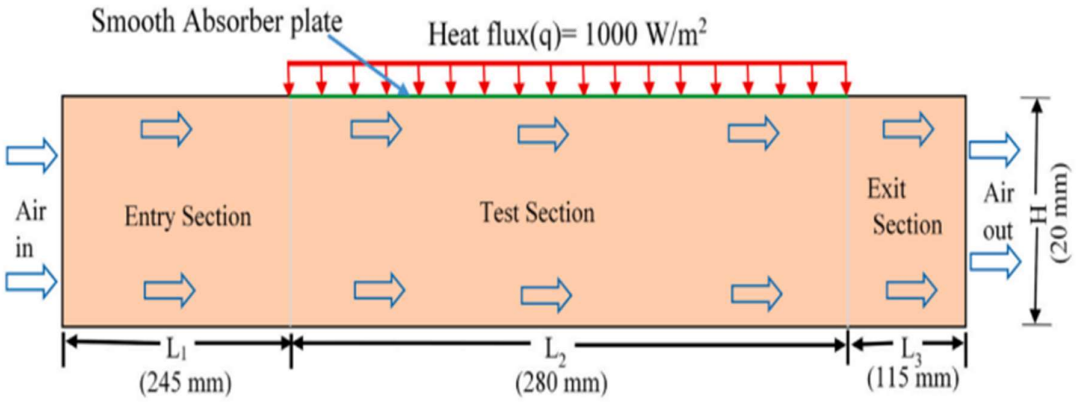

Fig. 3.1 Solar air heater with smooth absorber plate

The dimensions of geometry have been selected in accordance with ASHRAE Standard 93, 2003, which specifies the test procedures for steady-state or quasi-steady-state thermal performance testing. The fundamental justification for running the test in steady-state settings is to avoid transitory impacts that might exaggerate the measured performance of a collection. The **Fig. 3.2** presents the 3-D design of solar air heater. The following set of steady-state requirements is taken directly from the Standard's strict definitions:

a) **Solar irradiance:** According to ASHRAE 93-2003, a surface's globally averaged sun irradiance must be at least 790 W/m^2 to be normal to the direct beam radiation. On the collection plane, a solar irradiance fluctuation of no more than ±32 W/m^2 is permitted.

b) **Ambient Temperature:** For all data periods, the variation of ambient temperature must be less than 30°C.

c) **Flow Rate:** For all data points, the flow rate of the heat transfer fluid is constant. For a liquid fluid, a mass flow rate with an aperture area of 0.02 kg/s-m is advised. The flow rate must be kept constant within 0.000315 liters per second at the optimum flow rate.

d) **Inlet Temperature:** According to ASHRAE 93-2003, the input temperature during the test must be constant within +1°C or +1.8°F and it should be controlled within ±0.05°C or ±0.09°F.

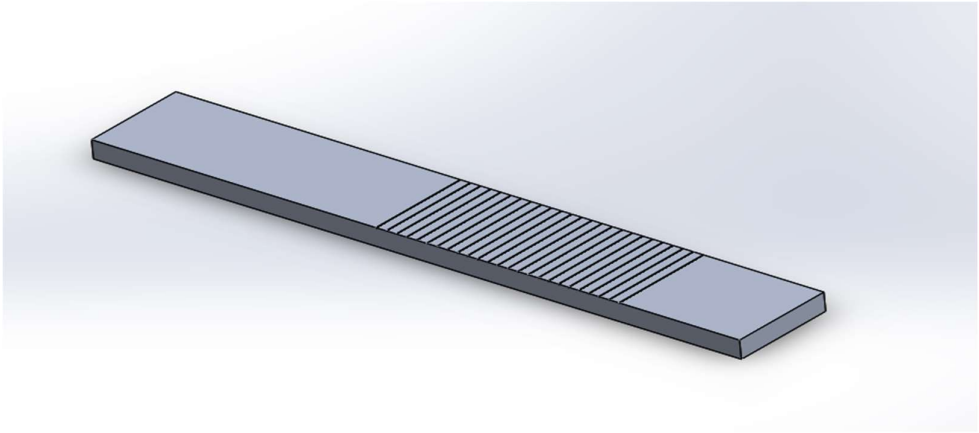

Fig. 3.2 3-D design of solar air heater with roughened absorber plate

3.2.1 Designing of model

The geometry of the selected obtuse- L roughness is shown in **Fig. 3.3**. The lower side of the absorber plate features an obtuse-L roughness as present in **Fig. 3.4**. There are three different types of roughness. The first kind is obtuse-L roughness shown in **Fig. 3.5**. The second type is opposite obtuse-L roughness as shown in **Fig. 3.6**, while the third type combines the first two in **Fig. 3.7** so a total of 3 designs are there. Pitch samples were taken in four different sizes (10mm, 15mm, 20mm and 25mm) with 6 Reynolds numbers ranging from 3800 to 18000 so a total of 72 design parameters are taken into consideration.

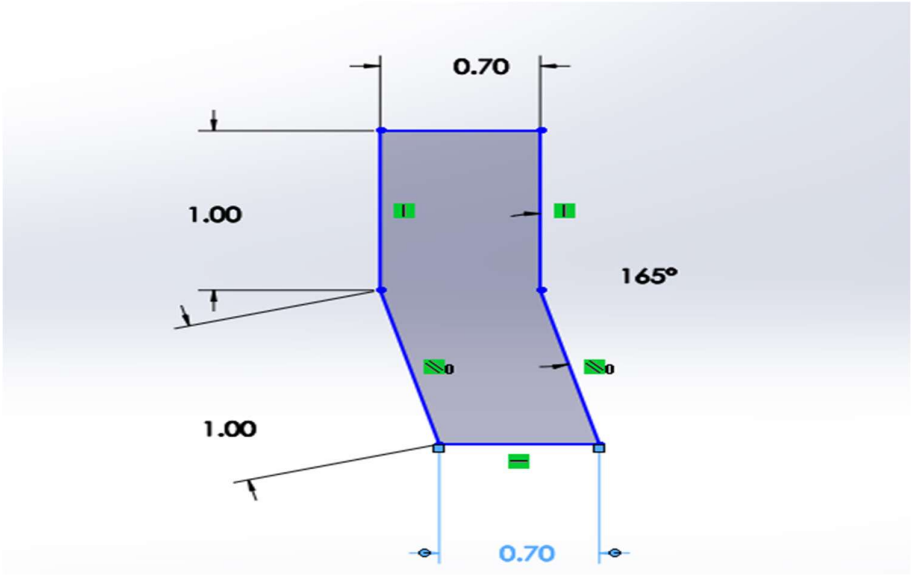

Fig. 3.3 Obtuse -L roughness profile

Fig. 3.4 Solar air heater having Obtuse-L roughness

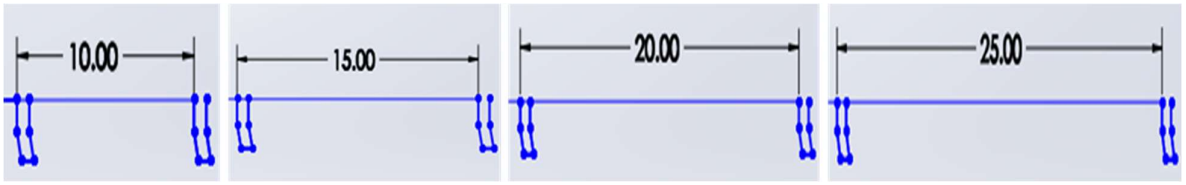

(a) (b) (c) (d)

Fig. 3.5 1st design parameters (a) 10mm pitch (b) 15mm pitch (c) 20mm pitch (d) 25mm pitch

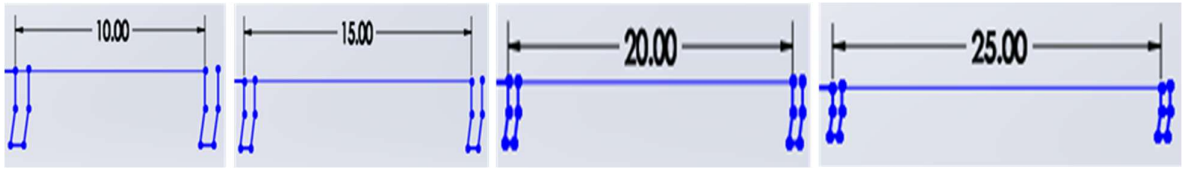

(a) (b) (c) (d)

Fig. 3.6 2st design parameters (a) 10mm pitch (b) 15mm pitch (c) 20mm pitch (d) 25mm pitch

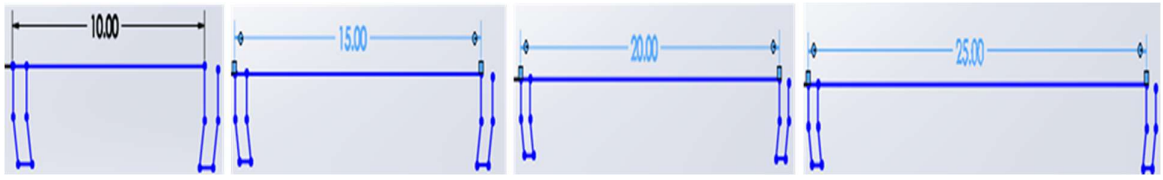

(a) (b) (c) (d)

Fig. 3.7 3rd design parameters (a) 10mm pitch (b) 15mm pitch (c) 20mm pitch (d) 25mm pitch

Table 3.1 consist of all the details regarding type of design, direction of flow and geometrical parameters (Roughness pitch, Reynolds number and Roughness angle) which are used as input to the software.

Table 3.1 Flow and geometrical parameters

S.No.	Type of Design	Desigh if roughness	Roughness Pitch	Reynolds number	Roughness angle
1.	Design-1	Obtuse-L	10 mm, 15 mm, 20 mm, 25 mm	3800, 5000, 8000, 12000, 15000, 18000	165°
2.	Design-2	Opposite obtuse-L			
3.	Design-3	Combination of both designs			

Air is the chosen fluid for examination, and aluminum is used as the collector plate of the solar air heater. The thermo-physical characteristics of the chosen materials as entered the ANSYS FLUENT solver are compiled in **Table 3.2** for the entire simulation set.

Table 3.2 Thermo- physical properties of the materials

	K (Thermal conductivity) (W/m-K)	**C_p or C (Specific heat) (J/Kg-K)**	**ρ (Density) (Kg/m^3)**	**μ (Dynamic viscosity) (Kg/m-s)**
Aluminum	202.4	871	2719	-
Air	0.0262	1007	1.117	1.857×10^{-5}

3.2.2 Grid Generation

The geometry was meshed, and a grid was generated using ANSYS ICEM. A two-dimensional quad mesh was generated as shown in **Fig. 3.8**. The smoothness was retained at a high level. Default value has been taken for growth rate and normal angle as 1.010 and 18° respectively. With a growth rate of 1.010, the default curvature normal angle was maintained at 18°. The transition ratio has been taken as 0.272. The skewness factor, aspect ratio, warp angle, Jacobian and orthogonal quality of the mesh parameters, which were maintained within desirable limits, are explained and presented on **Table 3.3** in the following subsections.

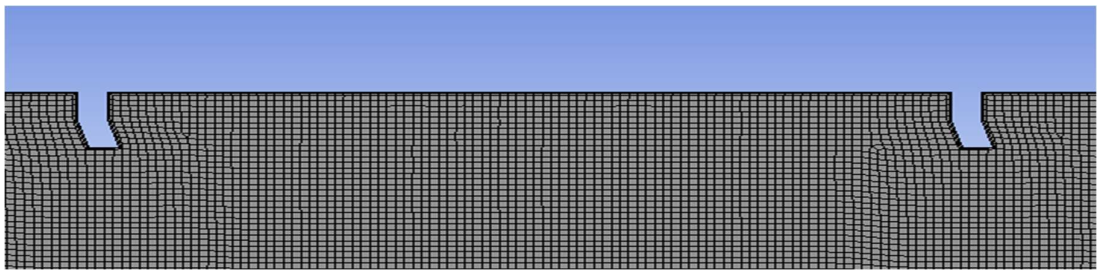

Fig. 3.8 Meshing of Obtuse-L roughness solar air heater

a) Skewness factor: It is the angular measurement of the cell. 0 has been taken as the perfect skewness value.

b) Aspect ratio: It is the ratio of minimum element edge length to maximum element edge length. The aspect ratio range is taken between 0 to 5. Value 0 is always taken as a recommendation and 5 is taken as the worst.

c) Orthogonal quality: It is another crucial cell characteristic on which convergence depends. In this, 1 stand for the highest-quality cell, and 0 for the lowest-quality cell.

d) Warp angle: Warp angle generally tells us whether all the elements are present on the same plane or not. 0^o warp angle taken an ideal and less than 10^o is acceptable.

e) Jacobian: Jacobian generally tells us by how much percentage our element is matching with an ideal mash. The ideal value of Jacobian is 1 and it is accepted as less than 0.6.

Table 3.3 Meshing parameters

S. No.	Parameters	Values	Range	Preferred value
1.	No. of elements	348797	-	-
2.	Element size	0.2 mm	-	-
3.	Element Quality	0.99995	0 to 1	1
4.	Aspect Ratio	2.8552	0 to 5	0
5.	Jacobian	1	0 to 1	1
6.	Warping factor	0	0 to 1	0
7.	Skewness	0.78333	0 to 1	1
8.	Orthogonal Quality	1	0 to 1	1

3.2.3 Grid Independence Test

Grid independence testing must also be done in addition to mesh quality checks in order to get more accurate findings as we reduce the cell size. The difference between the values must be taken into account during the grid independence test. When variations between the values become less than 1% then we have to stop more refined mesh. It is the most important test for getting the optimum size of the mesh.

$$\% \text{ Variation} = \left[\frac{\text{Previous value} - \text{Recent value}}{\text{Previous value}}\right] \times 100$$

The grid Independence Test for artificial roughness with design-1 and pitch is 10 mm at 18000 is presented in **Table 3.4**. It demonstrates unequivocally that there is little variance in the Nusselt number and friction factor values after 348797 elements. Thus, 348797 items were chosen for the study. The components in each configuration in the current analysis range from 400000 to 500000, depending on the pitch and roughness direction. There are 12 sets of geometries on which this parameter has been taken.

Table 3.4 Grid Independence Test

S. No.	Number of Elements	Nusselt Number (CFD)	% Variation in Nu	Friction Factor (CFD)	% Variation in f
1.	18560	63.04819	-	0.012107	-
2.	62714	70.94818	12.53008215	0.010836	-10.49805897
3.	94365	72.54717	2.253743507	0.010116	-6.644518272
4.	160497	73.60214	1.454184912	0.009987	-1.275207592
5.	225970	74.41611	1.105905345	0.009857	-1.3016922
6.	348797	74.91802	0.674464172	0.009877	0.202901491

3.2.4 Fluent Setup

During CFD simulations, ANSYS FLUENT is utilized to solve the equations. It contains too many numbers of governing equations. The mesh file is imported by the ANSYS FLUENT when meshing is completed in ANSYS ICEM (Integrated Computer-aided Engineering and Manufacturing). The problem setup, solution, and results are the three sections of the ANSYS FLUENT. The general, model, material, cell zone condition, boundary conditions, dynamic mesh, and reference values are all included in the problem setup. While solution consists of calculation activities, calculation module, solution initialization, solution controls, and solution methods. Finally, the graphics and animations, charts, and reports modules are listed under the results tab. There are some important setup tabs we have while going through ANSYS FLUENT.

a) General tab: It contains a mash check, from where we can check the mash parameter. Here we also have two types of solvers. These are Pressure based and density based. Pressure-based is used where the speed of the fluid is less than 1.3 Mach number and density based is used when the speed of the fluid is more than 1.3 Mach number. It

also has two types of velocity formulation. These are absolute and Relative. Absolute is used where the fluid is flowing and Relative is used where both domain and fluid are flowing. It also has 2 types of times. These are Steady and Transient steady state is taken where flow and flow characteristic does not change with respect to time whereas Transient is taken where flow and flow characteristic changes with respect to time.

b) Models tab: In the model tab we have to on the energy equation. An energy equation is used where there is heat transfer. There are various turbulence models available for simulating physiological problems, however, the optimal model for a particular issue must be chosen. The model must support the observed physical phenomena and the most appropriate model must be chosen, one that produces findings that are more similar to the experimental data. The physics of the phenomenon is better justified when there is a closer agreement with the experimental data. The same turbulence model that was used in **Yadav and Bhagoria's (2014)** study to validate it, k-ε RNG Enhanced wall treatment, is employed in this study as well since it adequately justifies the physical fact that **Yadav and Bhagoria (2014)** took into account when choosing their turbulence model. **Figs 3.9** and **3.10** display the model selection in ANSYS FLUENT.

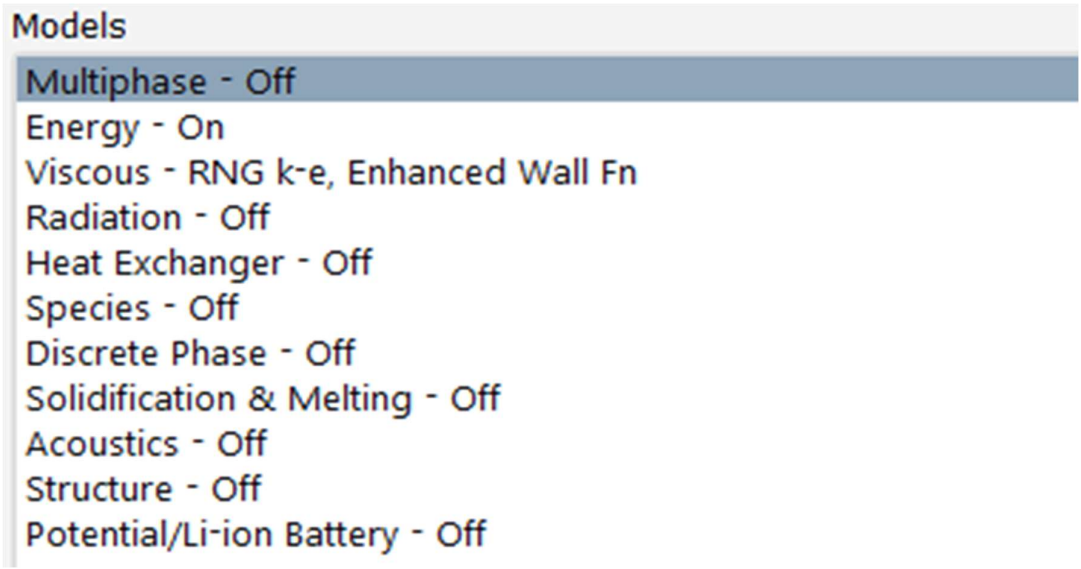

Fig. 3.9 Interface the models tab in ANSYS FLUENT

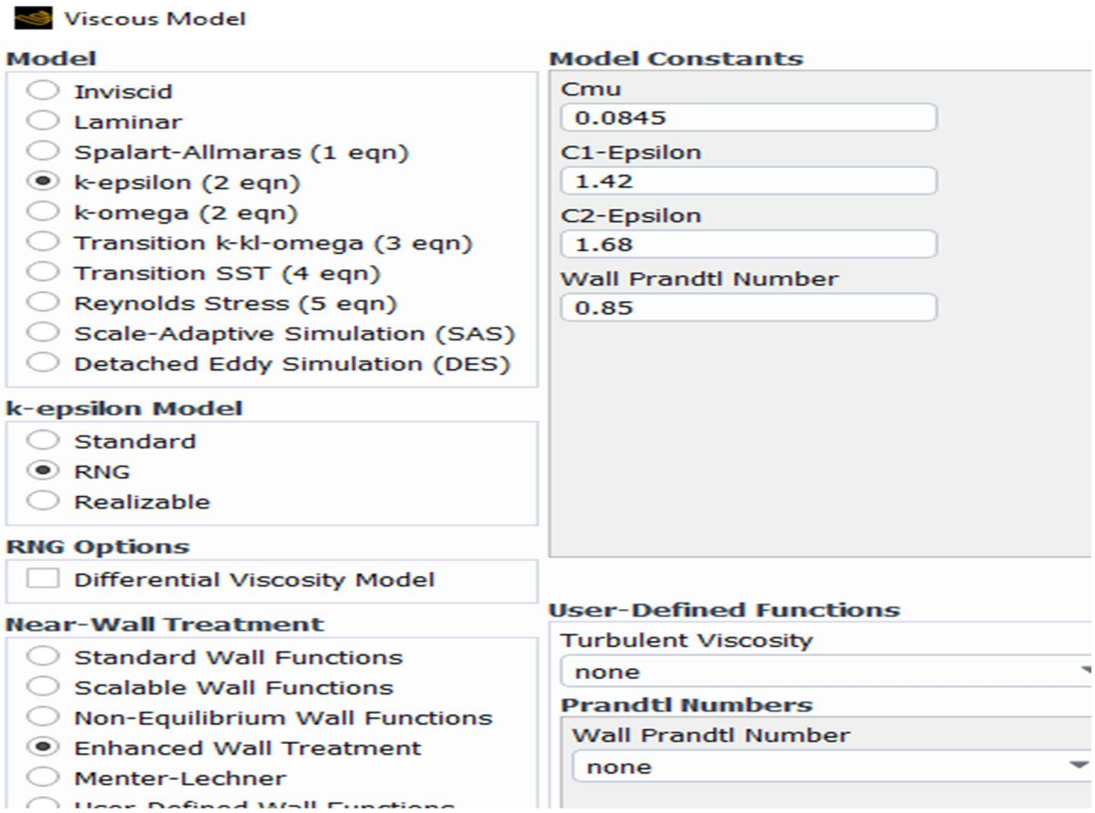

Fig. 3.10 Interface of selecting the perfect model

The Navier-Stokes equation, the Two-Dimensional continuity equation, and energy conservation are the three equations that govern models of airflow and heat transmission. Here are these equations:

Continuity Equation:

$$\frac{\partial}{\partial x_i}(\rho u_i) = 0 \tag{3.1}$$

Momentum Equation:

$$\frac{\partial}{\partial x_i}(\rho u_i u_j) = -\frac{\partial p}{\partial x_i} + \frac{\partial}{\partial x_j}\left[\mu\left(\frac{\partial u_i}{\partial x_j} + \frac{\partial u_j}{\partial x_i}\right)\right] + \frac{\partial}{\partial x_j}\left(-\partial u_i u_j\right) \tag{3.2}$$

Energy equation:

$$\frac{\partial}{\partial x_i}(\rho u_i T) = \frac{\partial}{\partial x_j}\left((\tau + \tau_t)\frac{\partial T}{\partial x_j}\right) \tag{3.3}$$

Where, τ is as molecular thermal diffusivity and τ_t is turbulent thermal diffusivity. These are also representing as:

$$\tau = \frac{\mu}{P_r} \quad \text{and} \quad \tau_t = \frac{\mu_t}{Pr_t}$$

Transport equations of k-ε model are:

$$\frac{\partial}{\partial t}(\partial k) + \frac{\partial}{\partial x_j}(\rho k u_j) = \frac{\partial}{\partial x_j}\left[(a_k \mu_{eff})\frac{\partial k}{\partial x_j}\right] + G_k + G_b - \rho\varepsilon - Y_M + S_k \quad (3.4)$$

$$\frac{\partial}{\partial t}(\rho\varepsilon) + \frac{\partial}{\partial x_j}(\rho\epsilon u_j) =$$

$$\frac{\partial}{\partial x_j}\left[(\alpha_\varepsilon \mu_{eff})\frac{\partial \varepsilon}{\partial x_j}\right] + C_{1\varepsilon}\frac{\varepsilon}{k}(G_k + C_{3G_k}G_b) - C_{2\varepsilon}\frac{\varepsilon^2}{k} - R_\varepsilon + S_\varepsilon \quad (3.5)$$

c) Boundary Condition: With the assist of the Reynolds number, the mean inlet velocity is calculated. "Velocity Inlet" condition has been used at the inlet and "Pressure Outlet" at the exit. It means at exit there is an atmospheric condition (1.013 x 10^5 Pa). The absorber plate has a "Uniform Heat Flux" with an applied heat flux of 1000 W/m^2. The inlet and outlet temperatures were taken to be 300 K. remaining walls has been taken as no slip boundary condition.

3.2.5 Solution method

"Residuals" are taken into consideration as a convergence criterion. For the continuity equation, the residual is in the scale of 10^{-3}, and for the energy equation, the residual is in scale of 10^{-6} in "Monitors", as shown in the **Fig 3.11**. The **Fig. 3.12** shows the Run Calculation tab in which number of iteration has been taken as 30000.

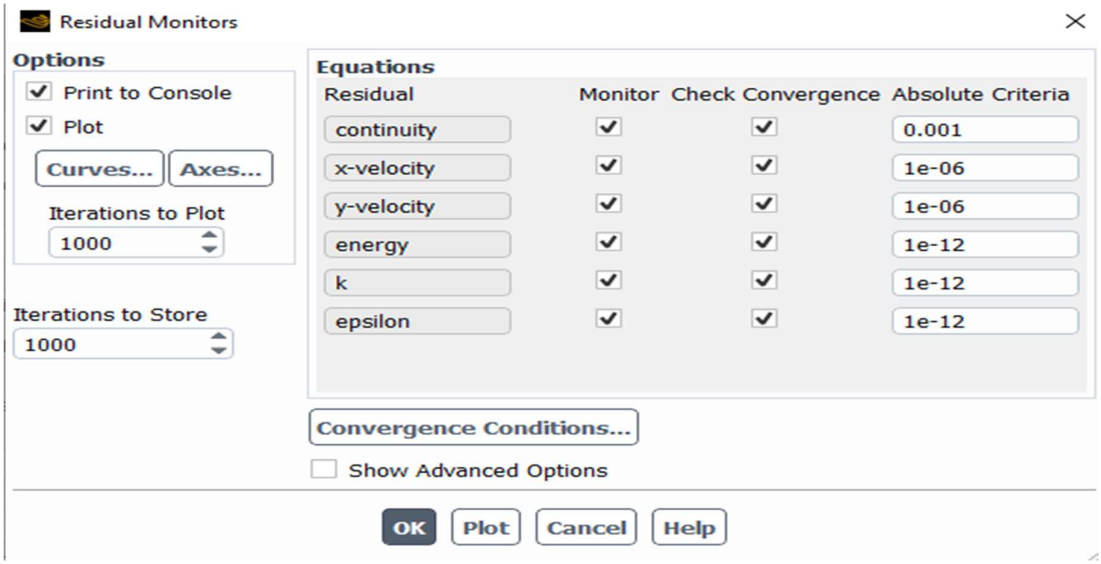

Fig. 3.11 Residual selection

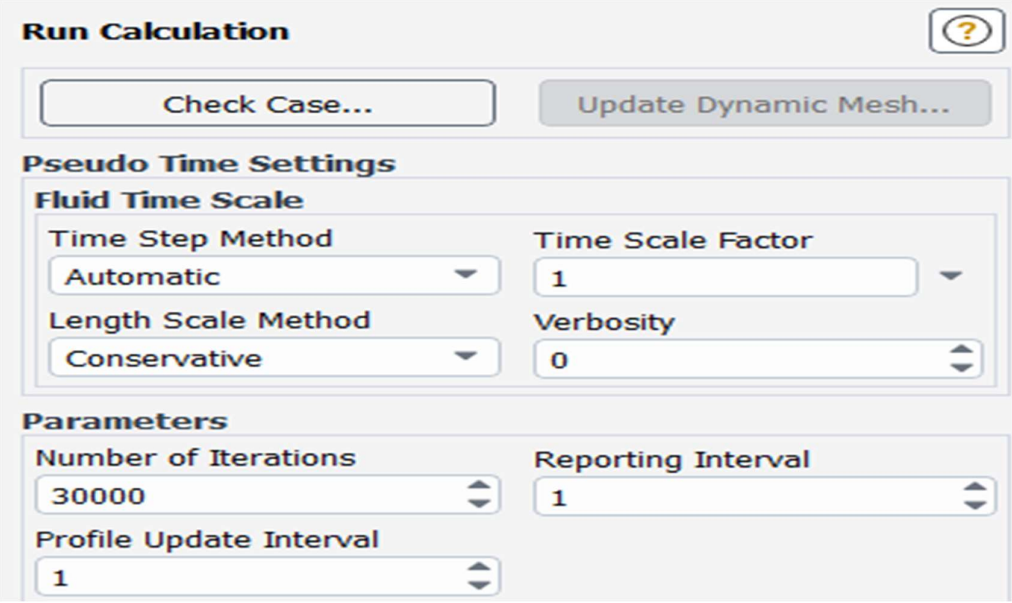

Fig. 3.12 Run calculation

After getting the values we just have to perform some mathematical calculation for getting to know the best design for our solar air heater. These calculations are shown as follow:

1. **Reynolds number (R_e):**

$$R_e = \frac{\rho v D_h}{\mu} \tag{3.6}$$

2. **Average heat transfer coefficient (h_{avg}):**

$$h_{avg} = \frac{\dot{m} c_p (T_{out} - T_{in})}{A_c (T_{mp} - T_{mf})} \tag{3.7}$$

$$T_{mf} = \frac{T_{in} + T_{out}}{2} \tag{3.8}$$

3. **Nusselt Number (Nu):**

$$(Nu_{avg})_r = \frac{(h_{avg} D_h)}{k} \tag{3.9}$$

4. **Friction factor (f_r):**

$$f_r = \frac{\Delta P . D_h}{2 \rho l v^2} \tag{3.10}$$

5. **Thermo-hydraulic performance parameter (THPP):**

$$THPP = \frac{\frac{Nu_r}{Nu_s}}{(\frac{f_r}{f_s})^{1/3}} \tag{3.11}$$

The "SIMPLE (semi-implicit method for pressure linked equation)" algorithm, developed by **Patankar (1980),** is employed for computing in the current work. For every transport equation, double precision solution is employed together with a second order upwind discretization approach.

The aforementioned method has been used to get the best design for the solar air heater. After preparing the model, meshing has been done. Some mathematical calculations have also done to get the desired values. These values help us for comparing the results in different parameters.

Resultsand Discussion

Chapter 4 RESULT AND DISCUSSION

4.1 General

Computational Fluid Dynamics (CFD) simulation was conducted in the flow domain of a solar air heater with an Obtuse - L roughness on the absorber plate. For changes in the Thermo hydraulic performance parameter, friction factor, and Nusselt number, the effects of pitch, roughness peaks, and Reynolds number are investigated. The change within Nusselt number, friction factor, and thermal-hydraulic performance parameter (THPP) are investigated in relation to the effects of pitch and Reynolds number.

The results of the Nusselt number, friction factor, and thermo-hydraulic performance parameter (THPP) were plotted against the Reynolds number and pitch. It has a significant effect on performance.

The result of the Blasius equation and the Dittus-Boelter equation for the smooth plate have been compared and validated in order to establish the validity of the suggested model. In order to ensure that the current model is valid, it has been also compared with the results of **Yadav and Bhagoria (2014)** taking into consideration their geometry. The subsections below provide more information on the validation and comparison.

4.2 Validation of Smooth absorber plate

Simulated outcomes for smooth absorber plate are compared with the **Yadav and Bhagoria (2014)**. For the aim of validating the friction factor and Nusselt number, respectively, the Blasius equation and the Dittus-Boelter equation are employed as conventional empirical correlations for the similar boundary and flow conditions.

4.2.1 Validation of Nusselt Number (Nu)

The results of **Yadav and Bhagoria (2014)** and Dittus-Boelter equation are compared with the Nusselt number values derived from computational fluid flow simulation. Dittus-Boelter equation is given for the Reynolds number ≥ 2300 and $0.7 \leq Pr \leq 160$:

$$Nu_s = 0.023\ Re^{0.8}\ Pr^{n} \tag{4.1}$$

Where,

n = 0.4 for heating (the plate temperature will be higher than fluid temperature)

n = 0.3 for cooling (the plate temperature will be lower than fluid temperature)

Fig. 4.1 shows a plot with the Nusselt number and Reynolds number for smooth absorber plate. It shows the comparison the CFD results with the standard results of Dittus-Boelter equation and **Yadav and Bhagoria (2014)**. The maximum deviation between CFD results and standard Dittus-Boelter equation is about ±9.07%.

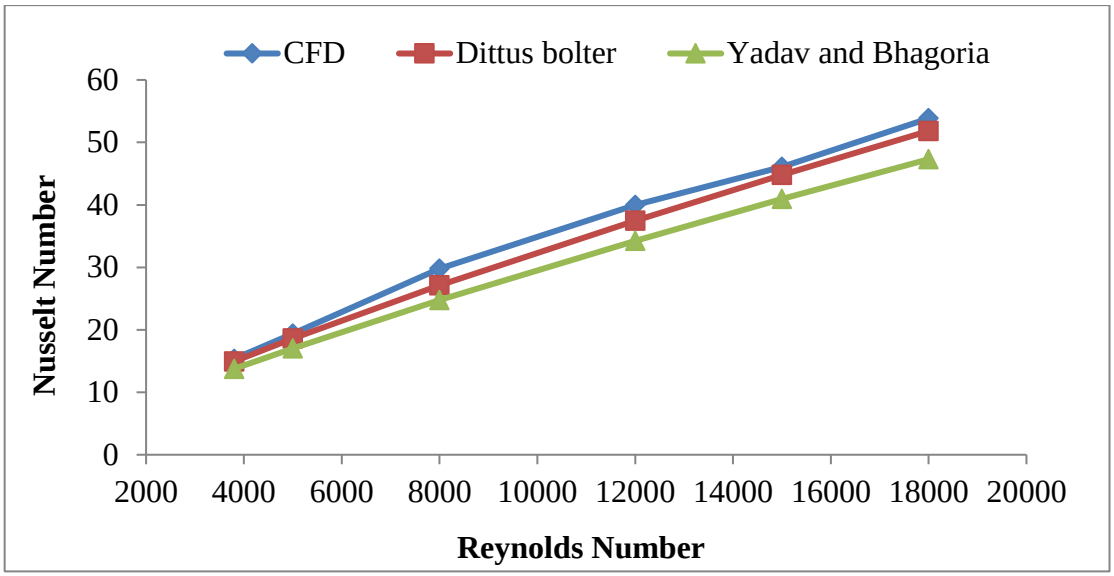

Fig. 4.1 Nusselt number against Reynolds Number (Smooth Absorber Plate)

The results of **Yadav and Bhagoria (2014)** for the square-shaped rib with a height of 1.4 mm and rib pitch roughness of 10 mm are also used to validate the Nusselt number shown in **Fig 4.2**. The maximum deviation between CFD and **Yadav and Bhagoria (2014)** results is about ±4.92%.

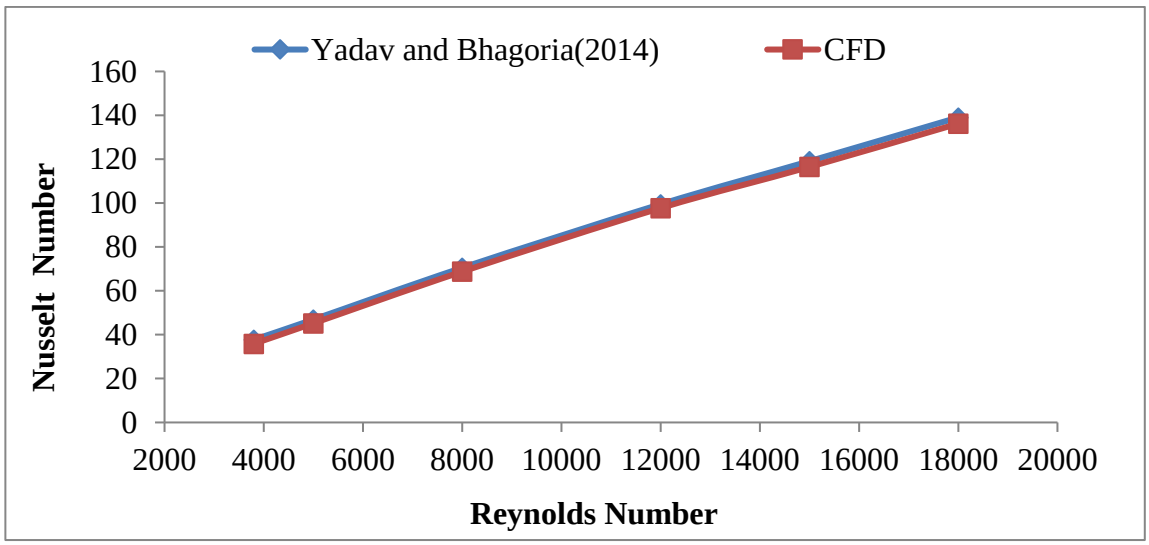

Fig. 4.2 Nusselt number against Reynolds Number (Rough Absorber Plate)

4.2.2 Validation of friction factor

The results of **Yadav and Bhagoria (2014)** and Blasius equation are compared with the friction factor values derived from computational fluid flow simulation. Equation 4.2 shows the Blasius equation:

$$f_s = 0.0791\ Re^{-0.25} \qquad \text{for } 2000 \leq Re \leq 100000 \qquad (4.2)$$

Fig. 4.3 shows a plot with the friction factor and Reynolds number for a smooth absorber plate. It shows the comparison the CFD results with the standard results of the Blasius equation and **Yadav and Bhagoria (2014)**. The maximum deviation between CFD results and standard Blasius equation is about ±2.95%.

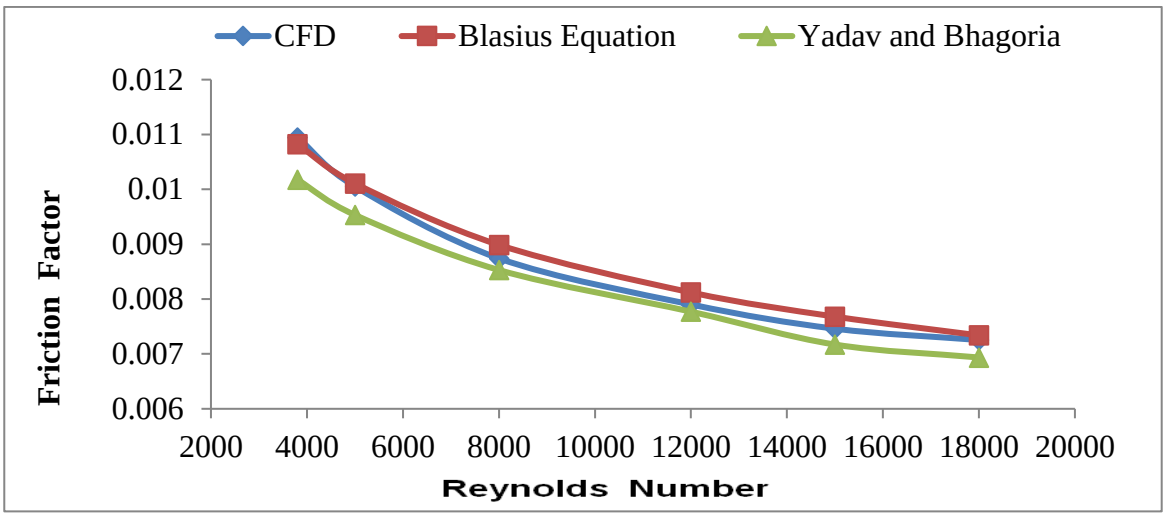

Fig. 4.3 Friction Factor against Reynolds number (Smooth Absorber Plate)

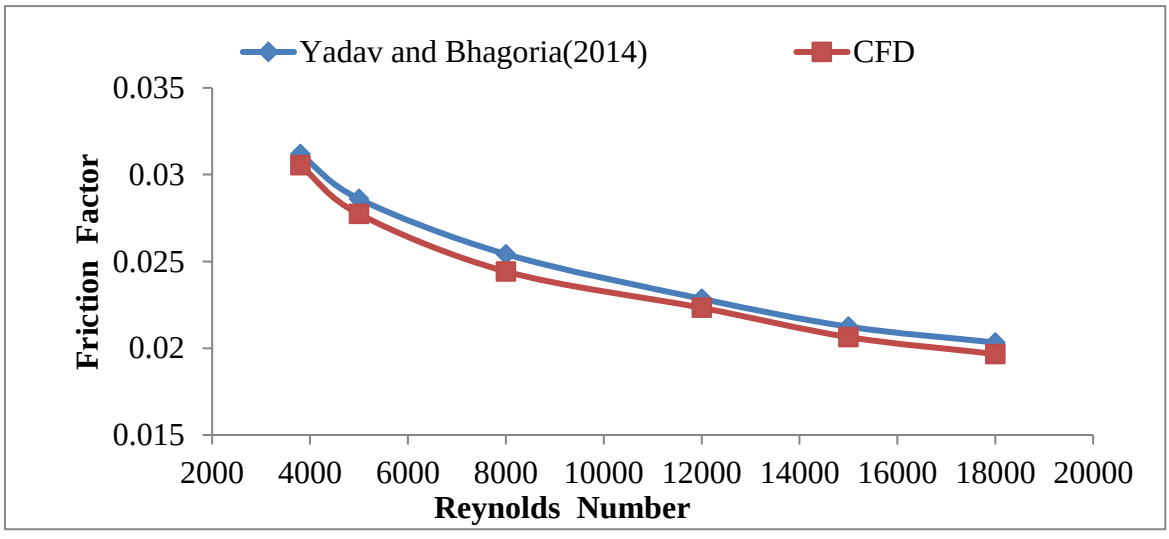

Fig. 4.4 Friction Factor against Reynolds number (Rough Absorber Plate)

The results of **Yadav and Bhagoria (2014)** for the square-shaped rib with a height of 1.4 mm and rib pitch roughness of 10 mm are also used to validate the Nusselt number shown in **Fig 4.4**. The maximum deviation between CFD and **Yadav and Bhagoria (2014)** results is about ±3.93%.

4.3 Variation in Nusselt number at different angles

Figure 4.5 shows the plot between the Nusselt number and Reynolds numbers at different angles. For this purpose, I have considered design-2, where the flow of air is the opposite direction of roughness inclination. Rib Pitch in taken as 10mm. For getting the best Obtuse-L angle, I have taken 7 different angles as 90^o, 105^o, 120^o, 135^o, 150^o, 165^o and 180^o in the interval of 15^o. Angle 165^o has the highest temperature at an outlet in the same configuration. After calculating the results, it can be seen that 165^o angle have the highest Nusselt number value. This is happening because 165^o helps to increase the Turbulence and reduces the heat accumulation between the ribs which causes reduce the laminar-sub layer and higher heat transfer between the absorber plate and air. And we get a maximum higher value of Nusselt number.

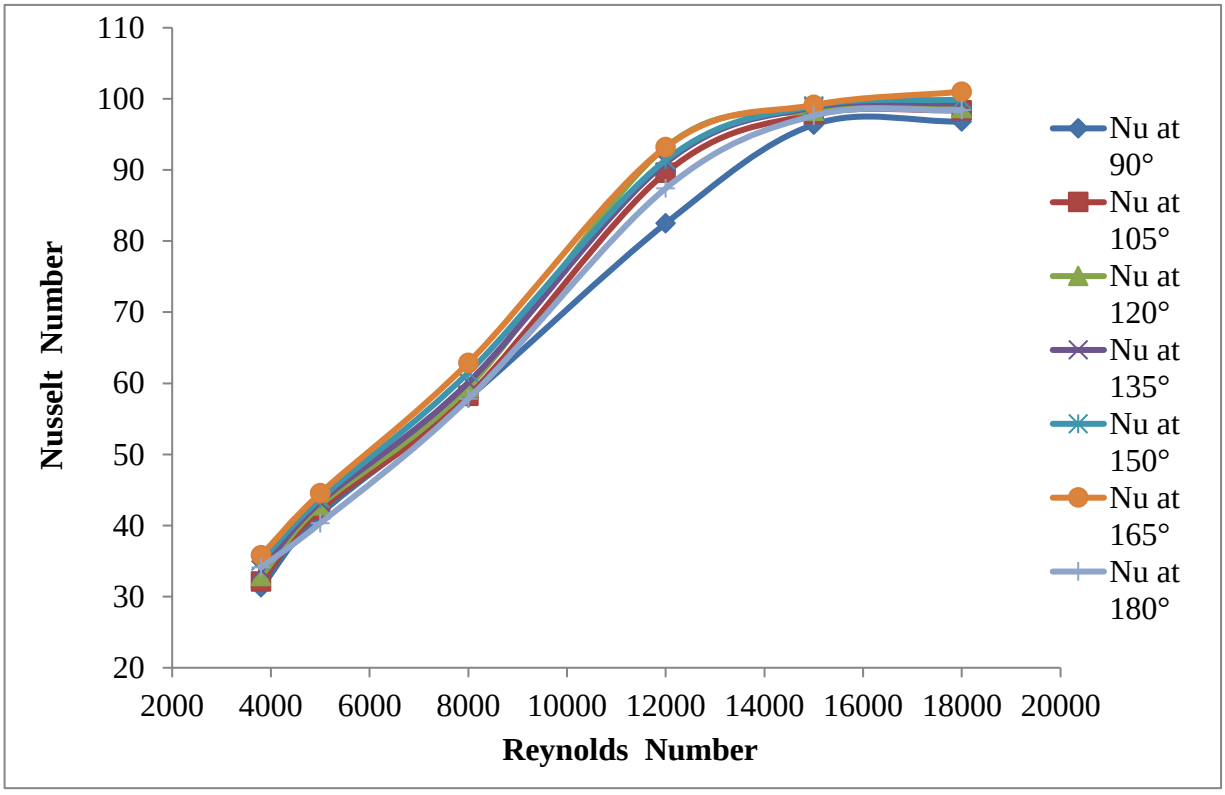

Fig. 4.5 Nusselt Number against Reynolds Number at Different angles

4.4 Variations in temperature throughout the absorber plate

The result obtained from the simulation presented in color filled graphical form. The **Fig. 4.6** show the temperature variation on the smooth surface and **Fig. 4.7** shows temperature variation in the roughed surface, **Fig. 4.8** shows velocity magnitude in design-3, **Fig. 4.9** show the turbulent kinetic energy and **Fig. 4.10** shows the turbulence intensity in design-3 at maximum velocity on a Reynolds number 18000.

The graphical representation shows clearly that roughened collection plates have a higher temperature gradient and outlet temperature than smooth collector plates. When looking in the direction normal to the collecting plate, the temperature gradient can be noticed. The cause of this can be understood by considering that the turbulence decreases near the collector as a result of the formation of a laminar sub-layer.

If we consider a fluid moving via a duct with a smooth absorber plate, the fluid next to the collector plate is observed to be at a higher temperature because the absorber plate is receiving a constant heat flux, but the convective heat transfer for smooth plates is constrained by the low turbulence and low-velocity turbulence in the close region of the plate. While the roughened absorber plate successfully breaks the laminar sub-layer. Additionally, because to the obstruction of the airflow caused by the roughened plate, there is comparably more turbulence and mixing of the air nearby which is increasing the rate of heat transfer. **Yadav and Bhagoria (2014)** also noted the related phenomena in their investigation of square-shaped ribs. Heat transfer has increased overall because of the increasing value of the heat transfer coefficient in the case of a roughened collector plate.

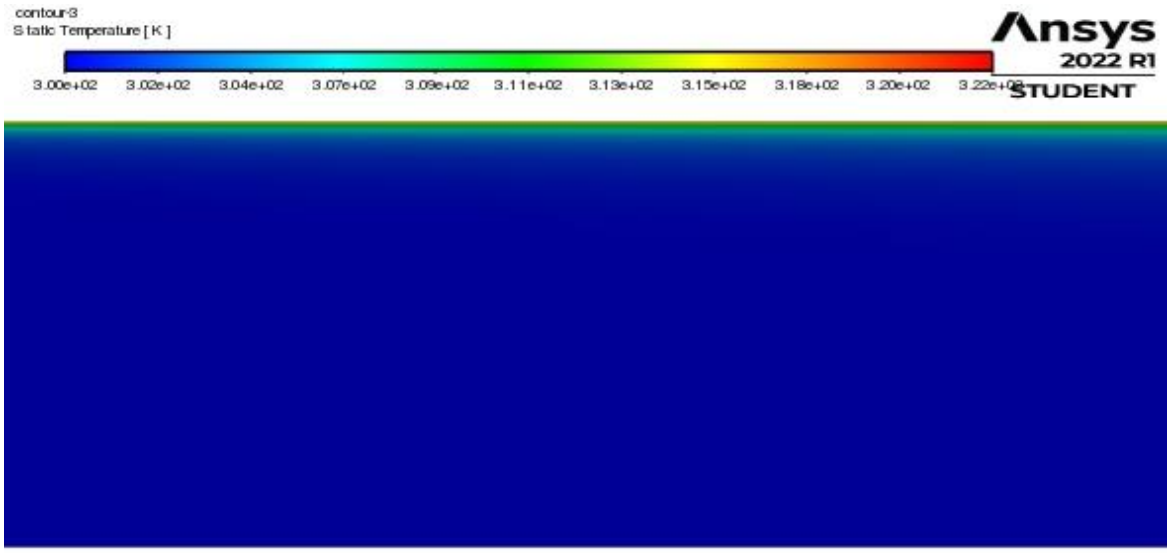

Fig. 4.6 Temperature distribution in smooth collector plate

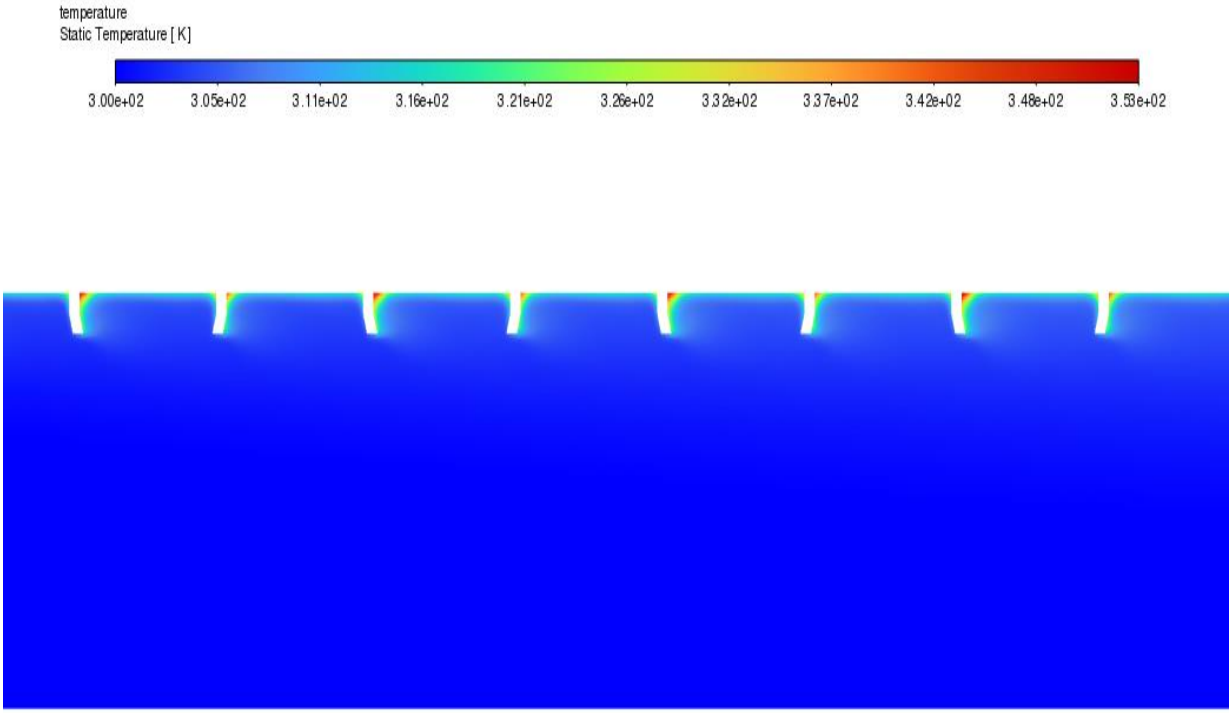

Fig. 4.7 Temperature distribution in design -3

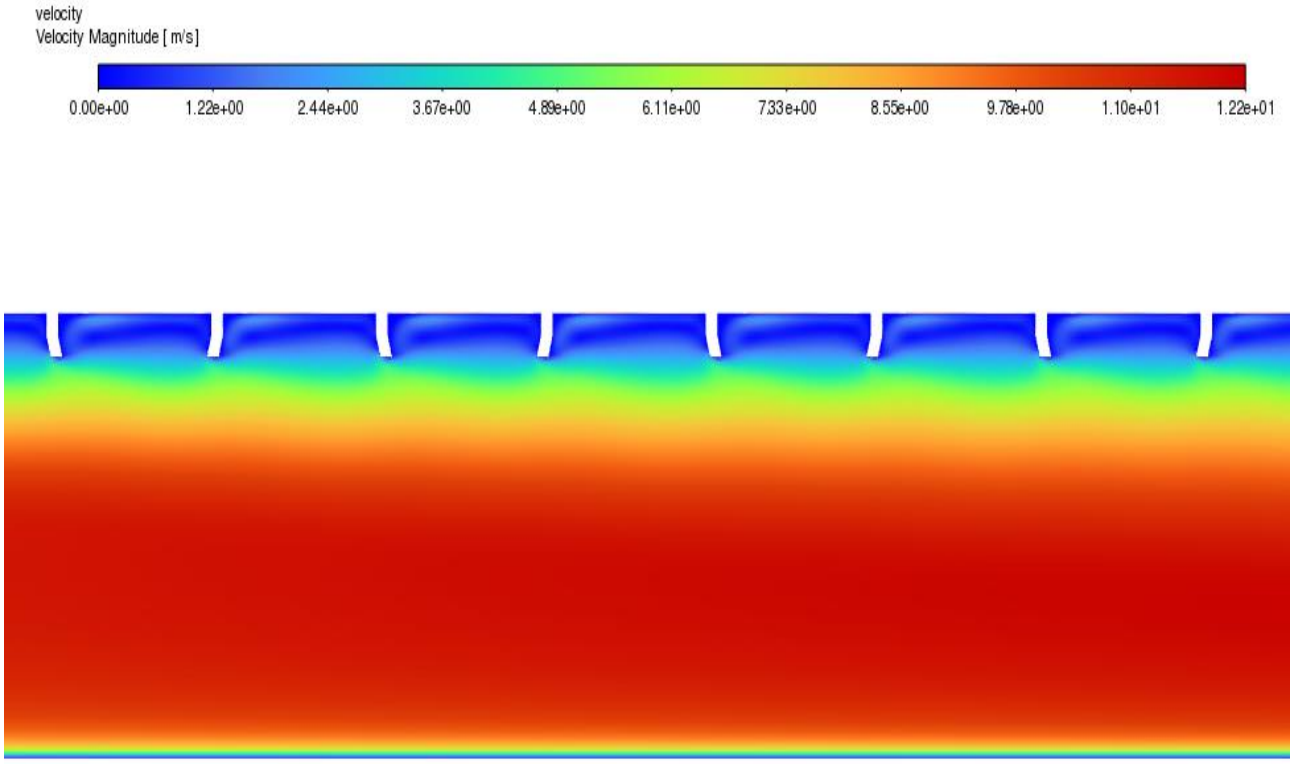

Fig. 4.8 Velocity magnitude in design -3

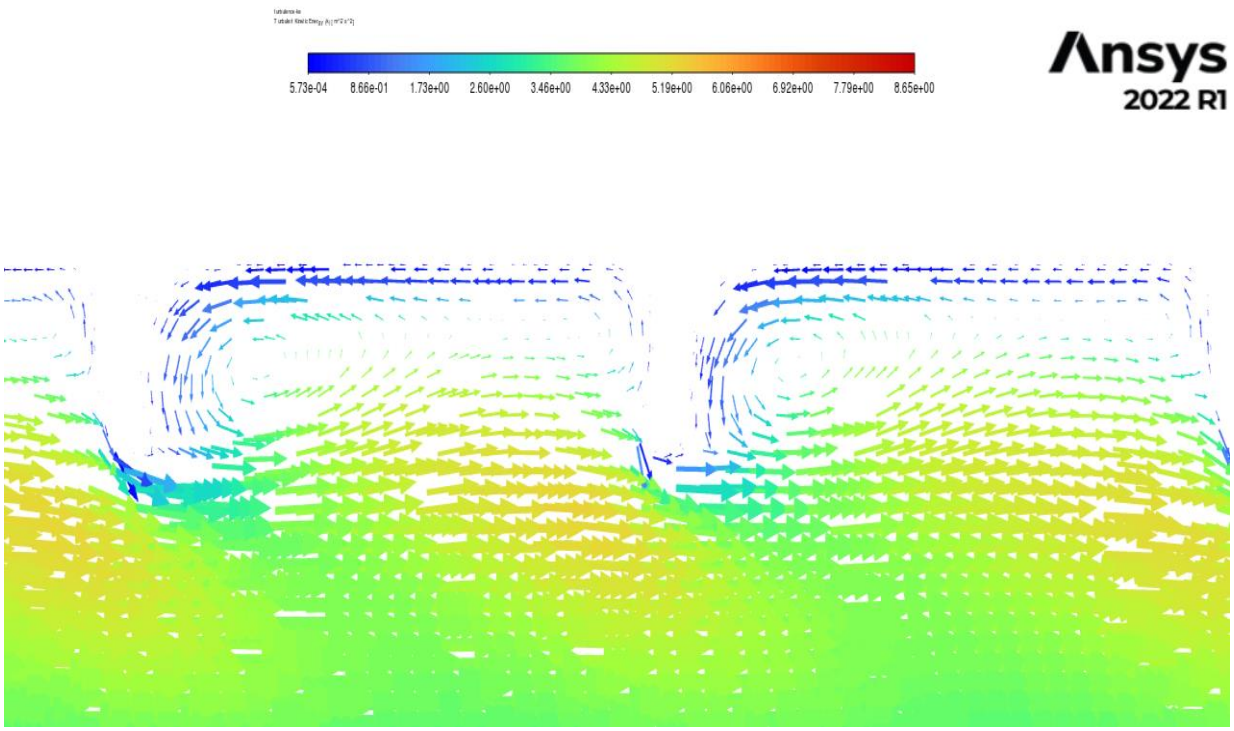

Fig. 4.9 Turbulence kinetic energy in Design -3

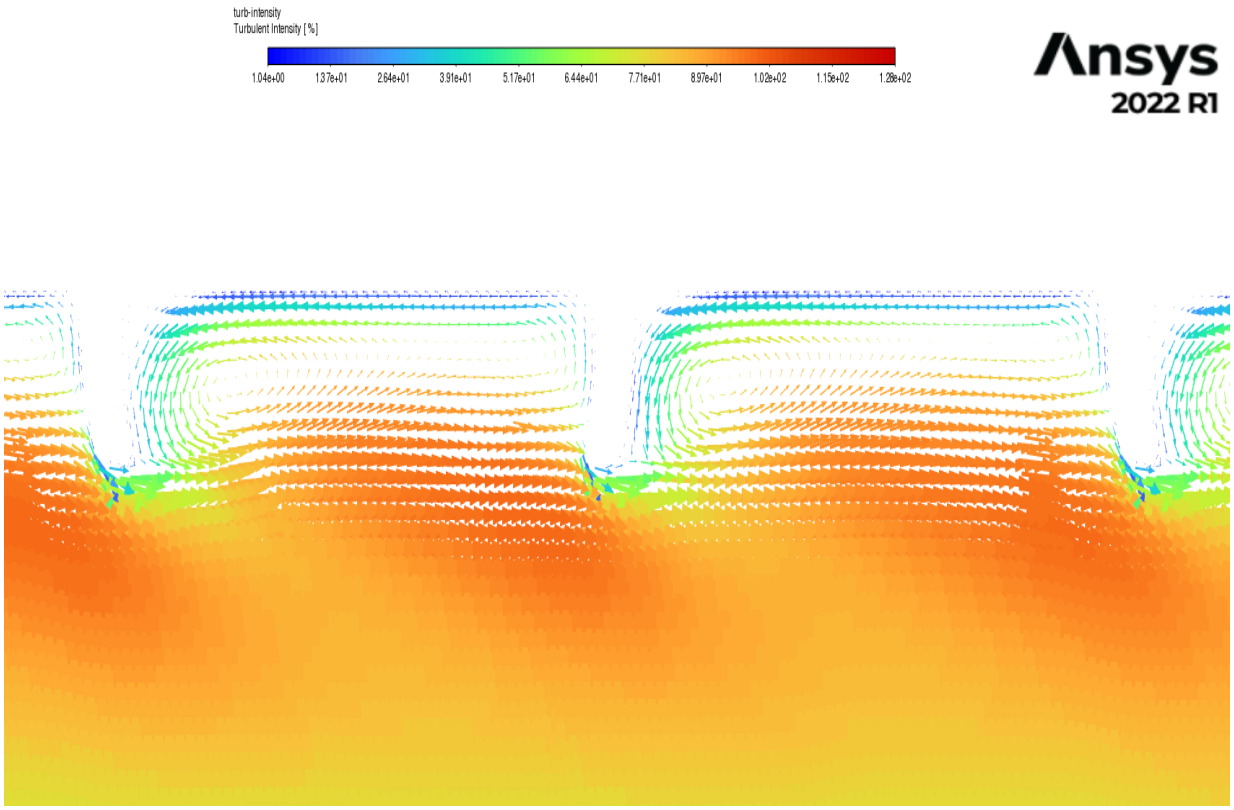

Fig. 4.10 Turbulence intensity in Design -3

4.5 Effect of Nusselt number

Fig 4.11, 4.12, and **4.13** show the plot between the Nusselt number and the Reynolds number. It can be seen from the plots that after the increases in the Reynolds number there is continuous increase in the Nusselt number for each value of rib pitch.

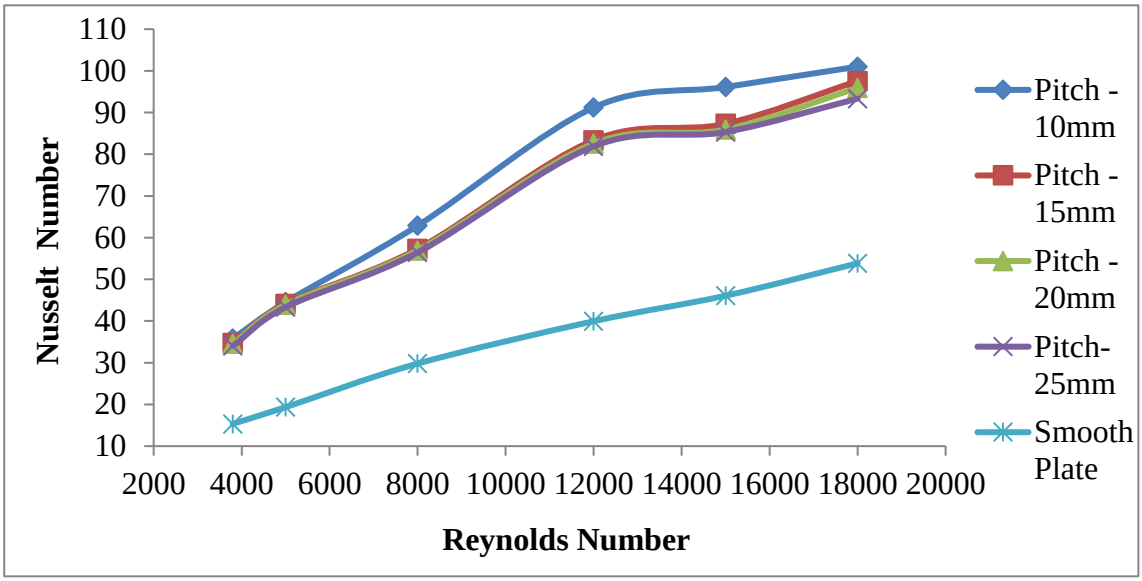

Fig. 4.11 Nusselt Number against Reynolds Number at Design -1

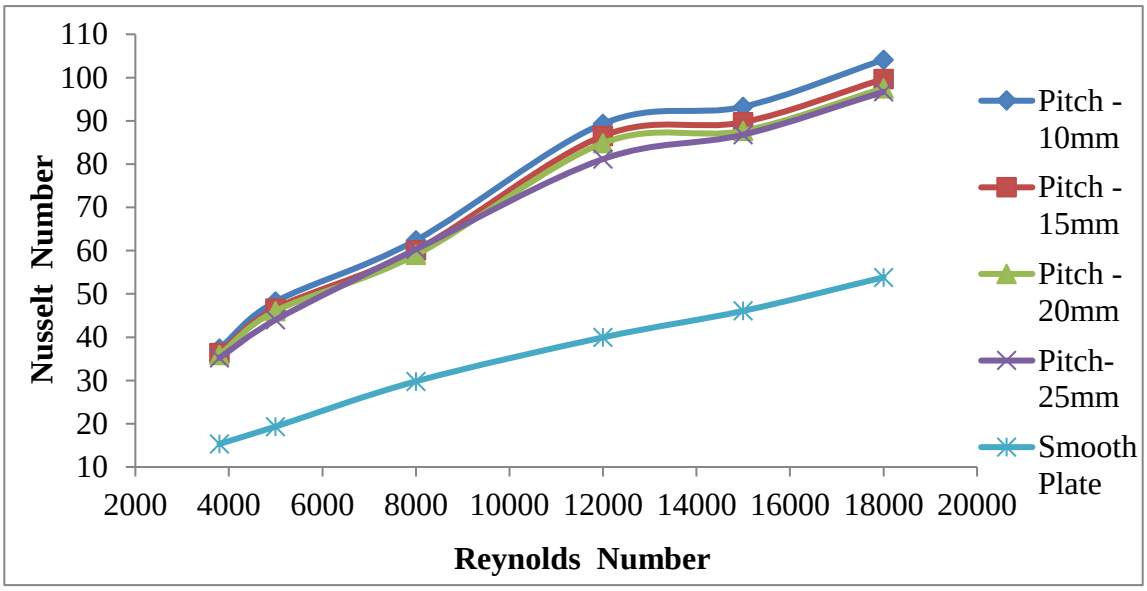

Fig. 4.12 Nusselt Number against Reynolds Number at Design -2

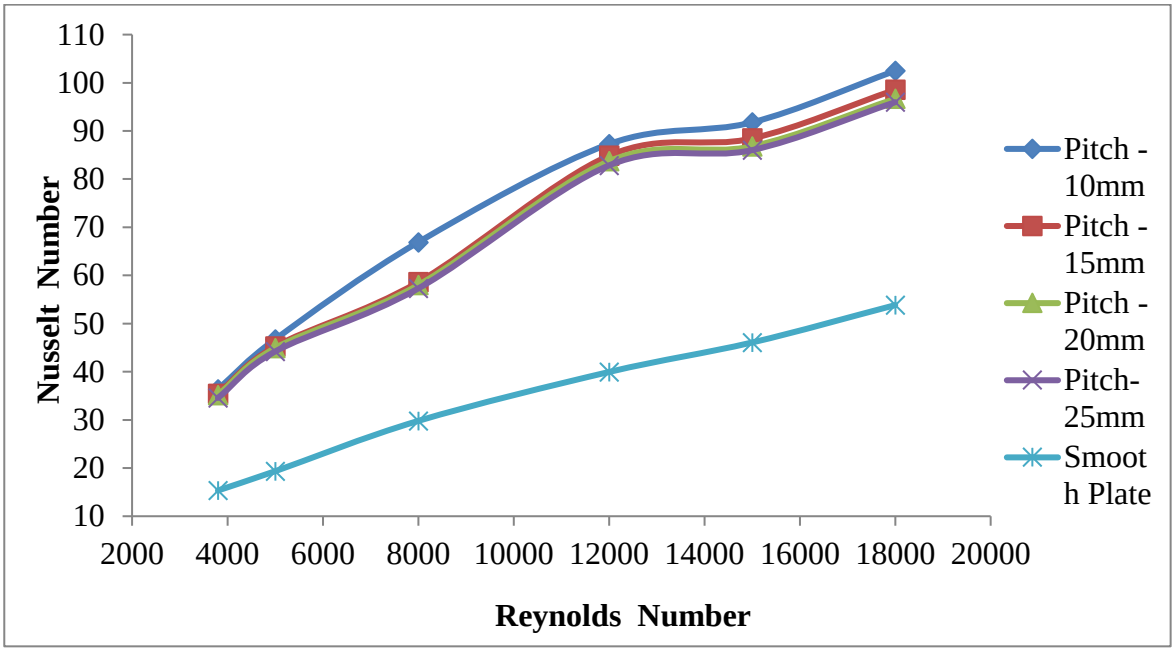

Fig. 4.13 Nusselt Number against Reynolds Number at Design -3

Also, the same results are also plotted between Nusselt numbers and Pitch keeping the fixed value of Reynolds number in **Fig. 4.14**, **4.15,** and **4.16**.

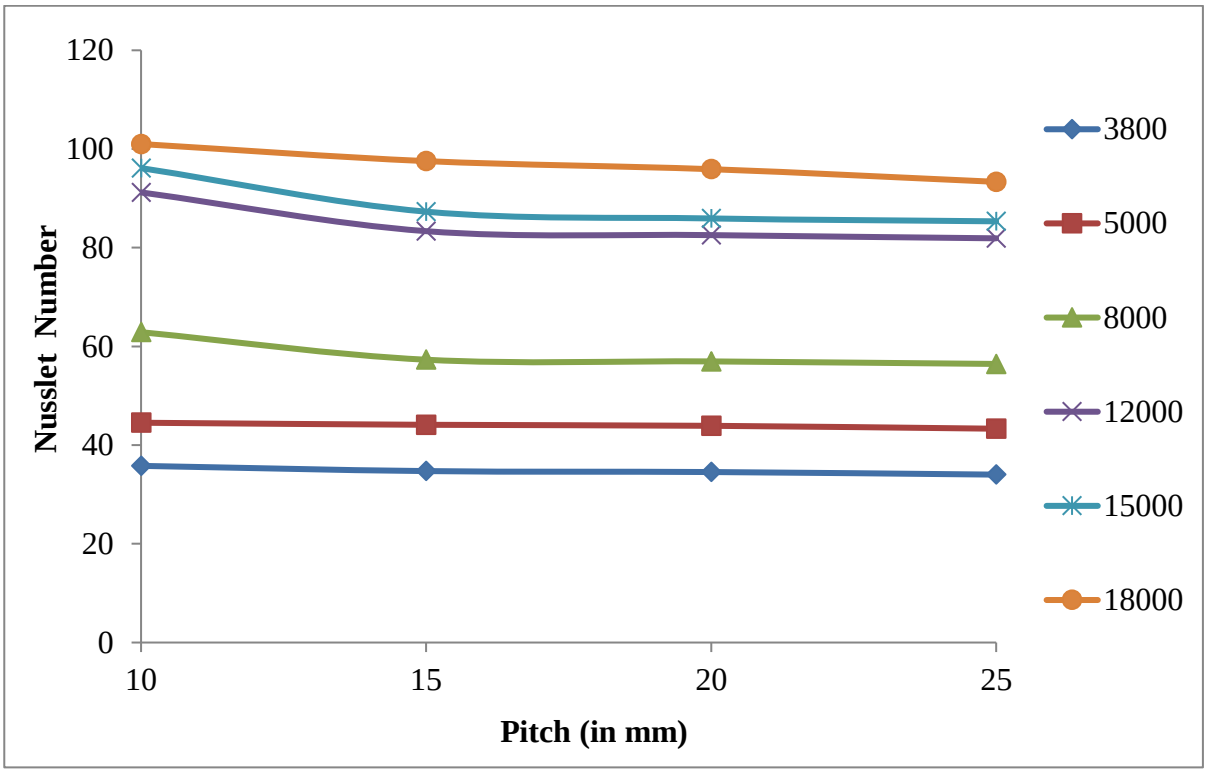

Fig. 4.14 Variation of Nusselt number against pitch at design-1

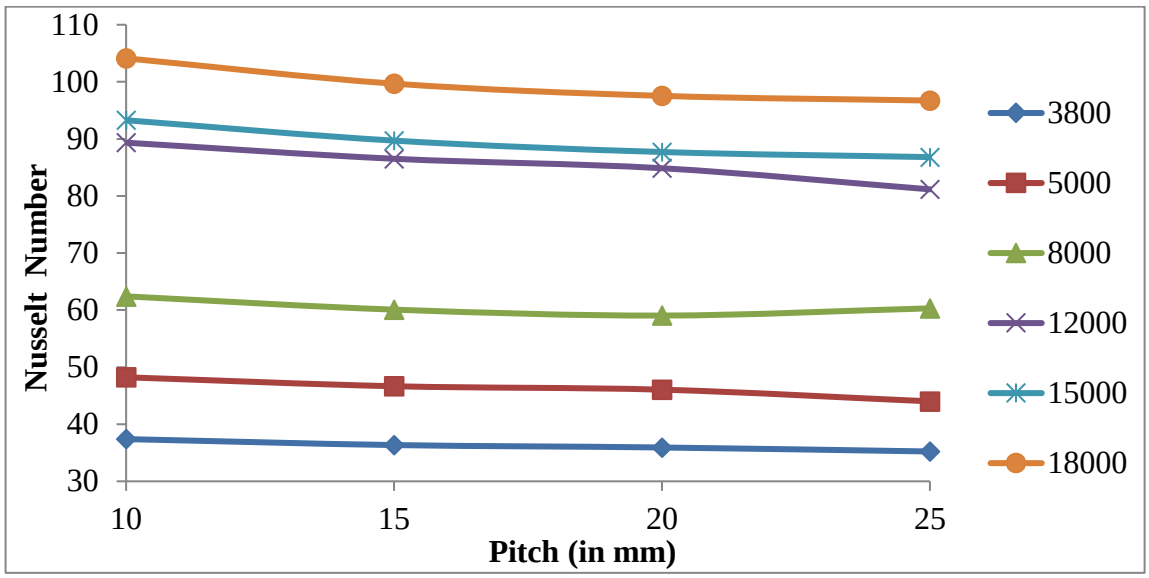

Fig. 4.15 Variation of Nusselt number against pitch at design-2

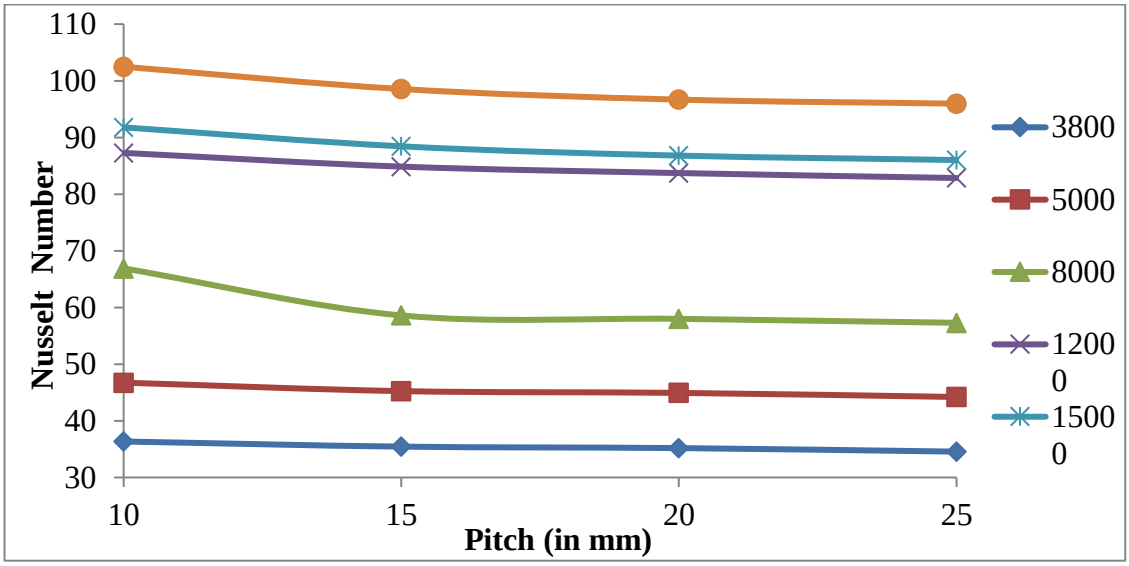

Fig. 4.16 Variation of Nusselt number against pitch at design-3

It can be concluded from the graphs that the Nusselt number value decreases at lower pitches and approaches constant values as the pitch value is increases. It also observes that while Reynold's number was smaller, the Nusselt number was also lower, and that when Reynolds' number increased, the Nusselt number increased as well. So, we can also conclude that Convective heat transfer decreases at lower Reynolds numbers and rises at higher Reynolds numbers.

The plots are generated as shown in **Figs. 4.17, 4.18,** and **4.19**. The enhancement ratio is also examined for the Nusselt number with regard to the values of the smooth plate. Plots demonstrate the improvement in heat transmission for various Reynolds

number levels. The figures show that, at first, the enhancement ratio increases more quickly as the Reynolds number increases, but that, after reaching a specific value of Reynolds number, the enhancement ratio almost decreases for design-1.

When the Nusselt Number enhancement factor in the case of design-2 rises from lower to higher Reynolds numbers and reaches its maximum at mid-values of Reynolds numbers, a decline may then be observed once more. Design- 3 also exhibits the same tendency.

This above-mentioned effect can be observed that Nusselt number enhancement rises from lower to higher values of Reynolds number at a certain limit and then it decreases. While the enhancement ratio values peak for greater values at Reynolds number values around 12,000. Initially, due to the lower Reynolds number and lower velocity, the transfer of heat is not much effective and the friction factor is also higher. As the Reynolds number increases, it increases the local disturbance near to the collector plate and which is able to transfer more heat and got a higher Nusselt number enhancement factor. When the Reynolds number is raised even further, it increases the turbulence which improves the heat transmission, but the pressure drop also rises more quickly, which reduces the value of the Nusselt number enhancement factor. In the current study, the Reynolds number of 12000 corresponds to the maximum value of Nusselt number enhancement factor.

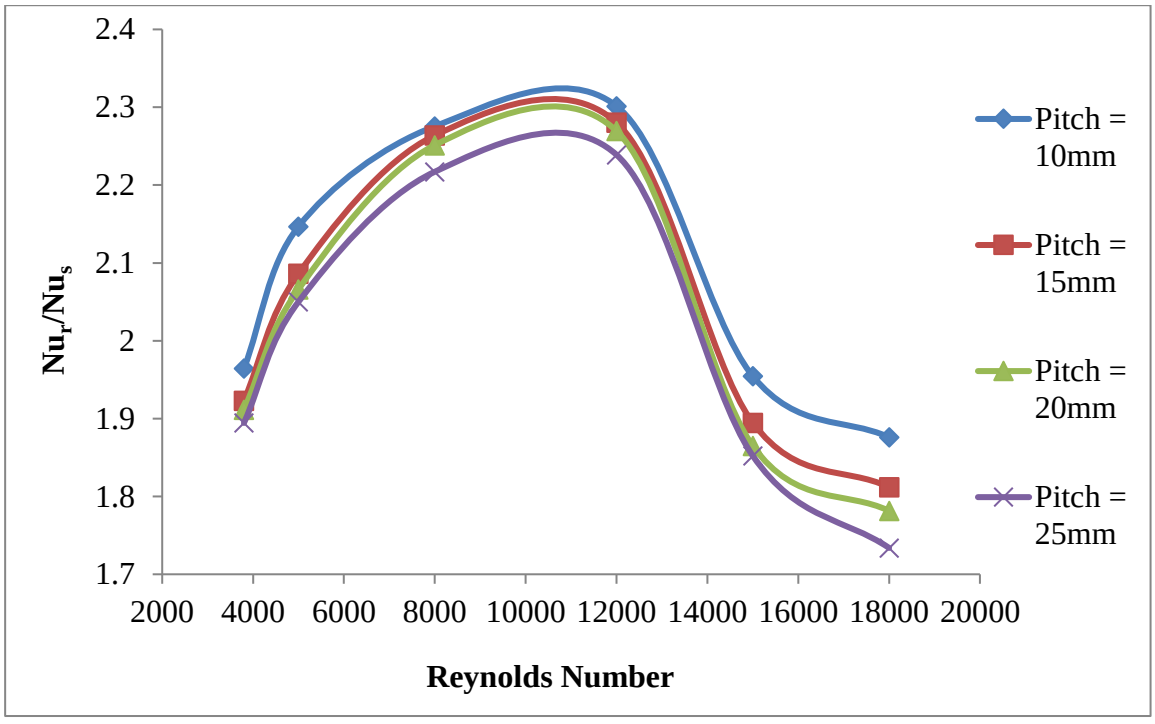

Fig. 4.17 Nusselt number enhancement factor against Reynolds Number at design- 1

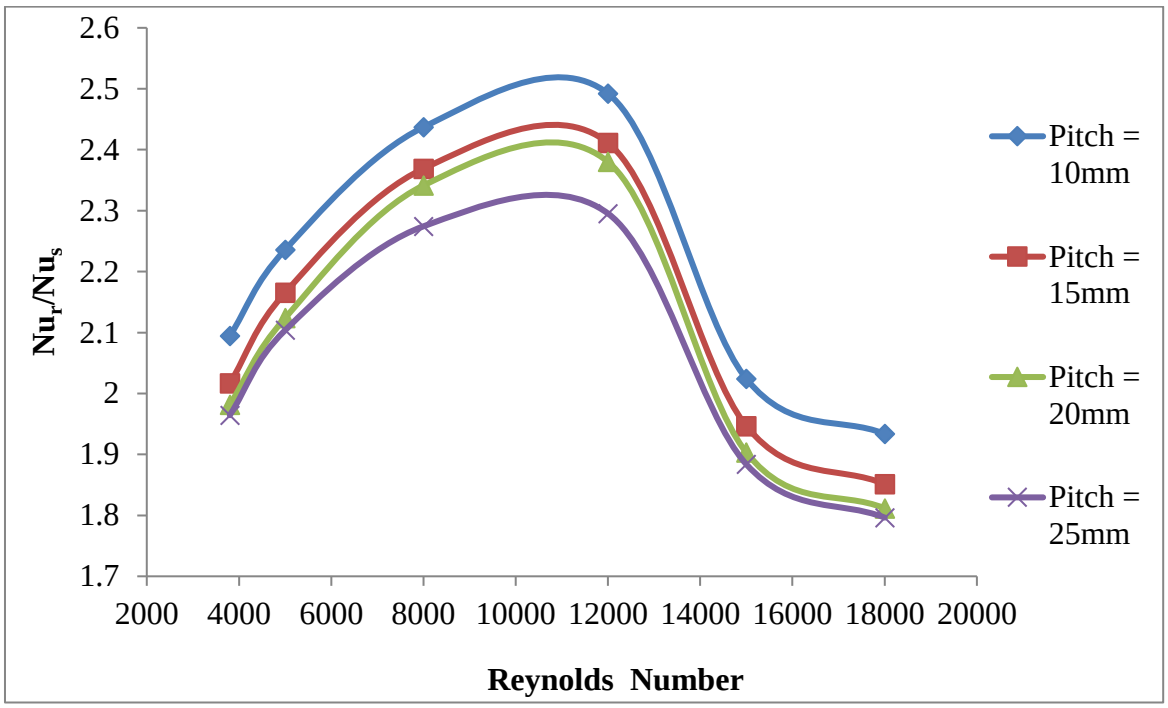

Fig. 4.18 Nusselt number enhancement factor against Reynolds Number at design- 2

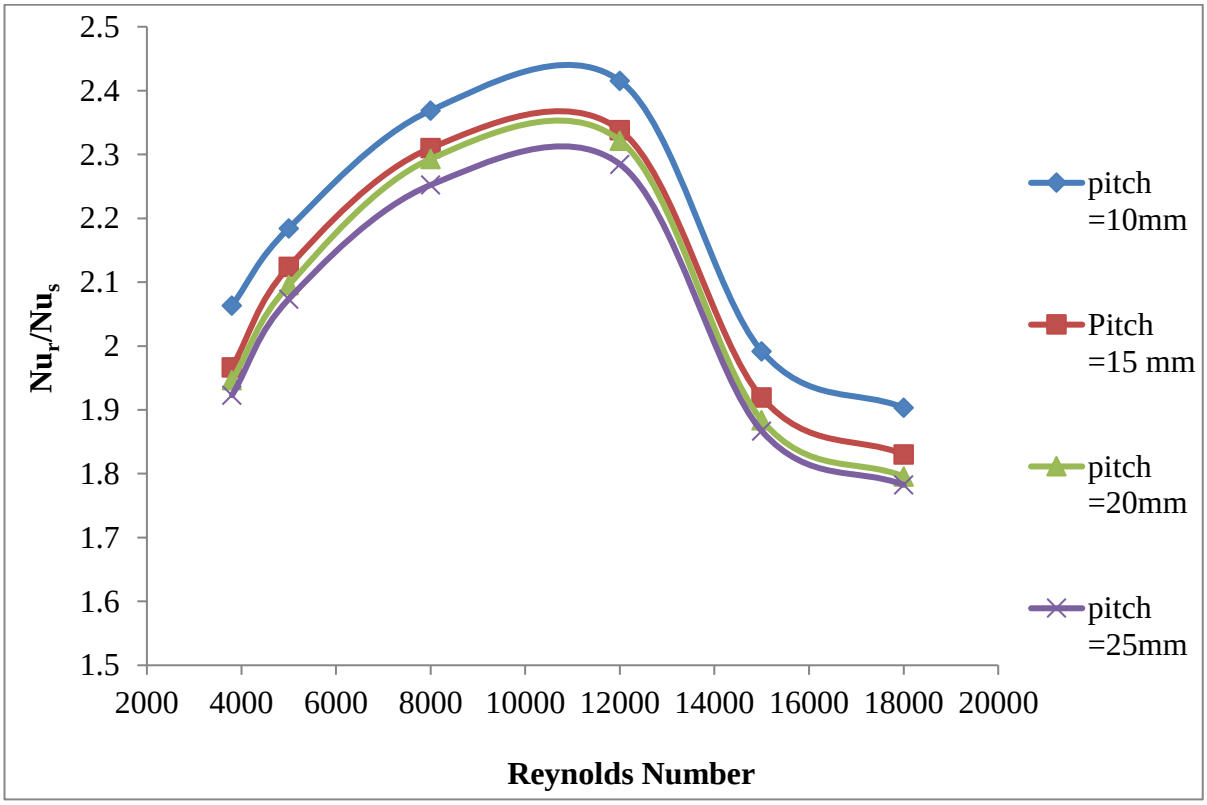

Fig. 4.19 Nusselt number enhancement factor against Reynolds Number at design- 3

4.6 Effect on Friction factor

Figures 4.20, 4.21, and **4.22** depict the friction factor vs. Reynolds number for various Reynolds number. As the Reynolds number rises, it is shown that the friction factor decreases for all pitch values. According to **Gawande et al. (2016)**, this phenomenon is characterized by the suppression of the laminar sublayer due to increasing mass flow rates. As flow rates increase, the thickness of the laminar sub-layer decreases due to increased turbulence.

In **Figs. 4.23, 4.24,** and **4.25**, graphs for friction factor against pitch over the various values of Reynolds number have been created to show the influence of pitch on friction factor. A higher friction factor is observed consistently to be associated with lower pitch values. Because lower-pitch geometries have more uneven surfaces than higher-pitch geometries, the friction factor reduces as the pitch increases. Therefore, the flow becomes more disrupted with lower pitch geometries, increasing pumping power loss.

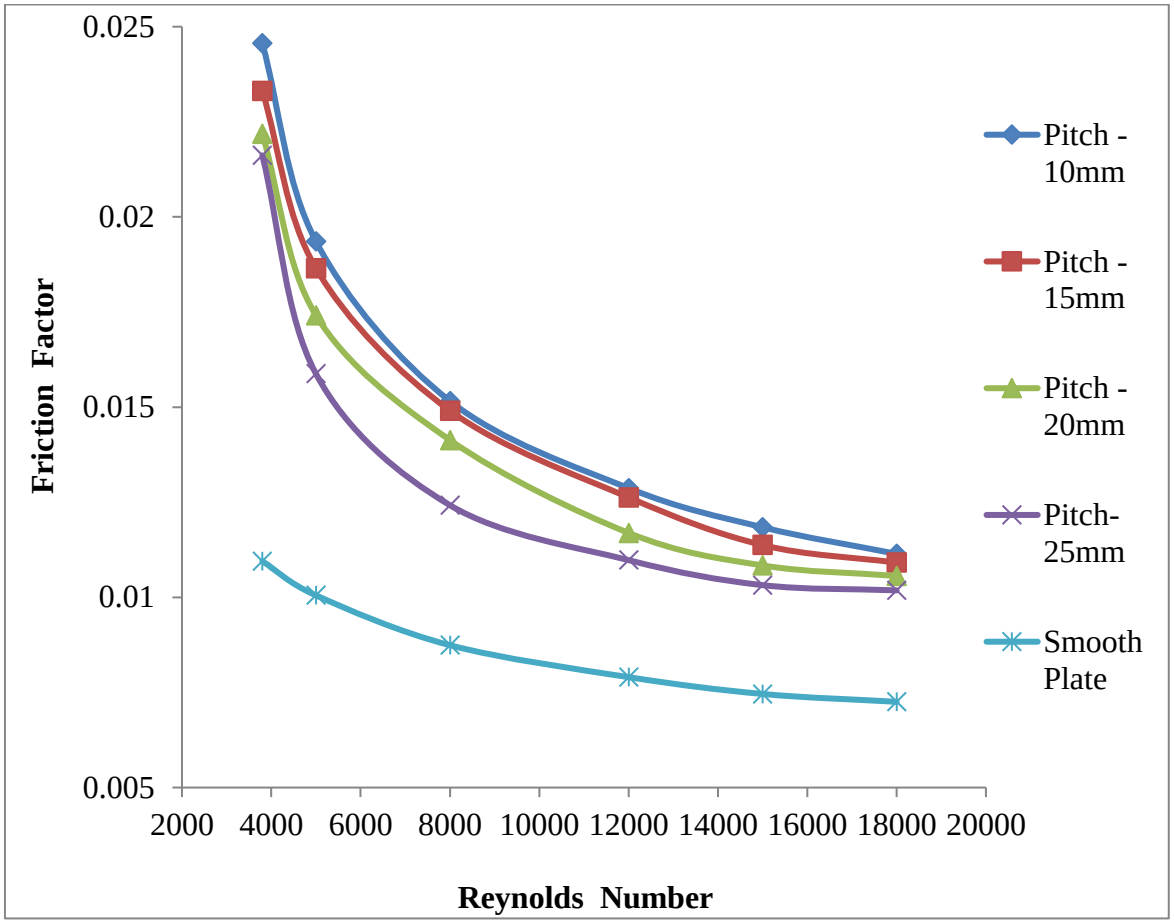

Fig. 4.20 Friction factor against Reynolds Number at design-1

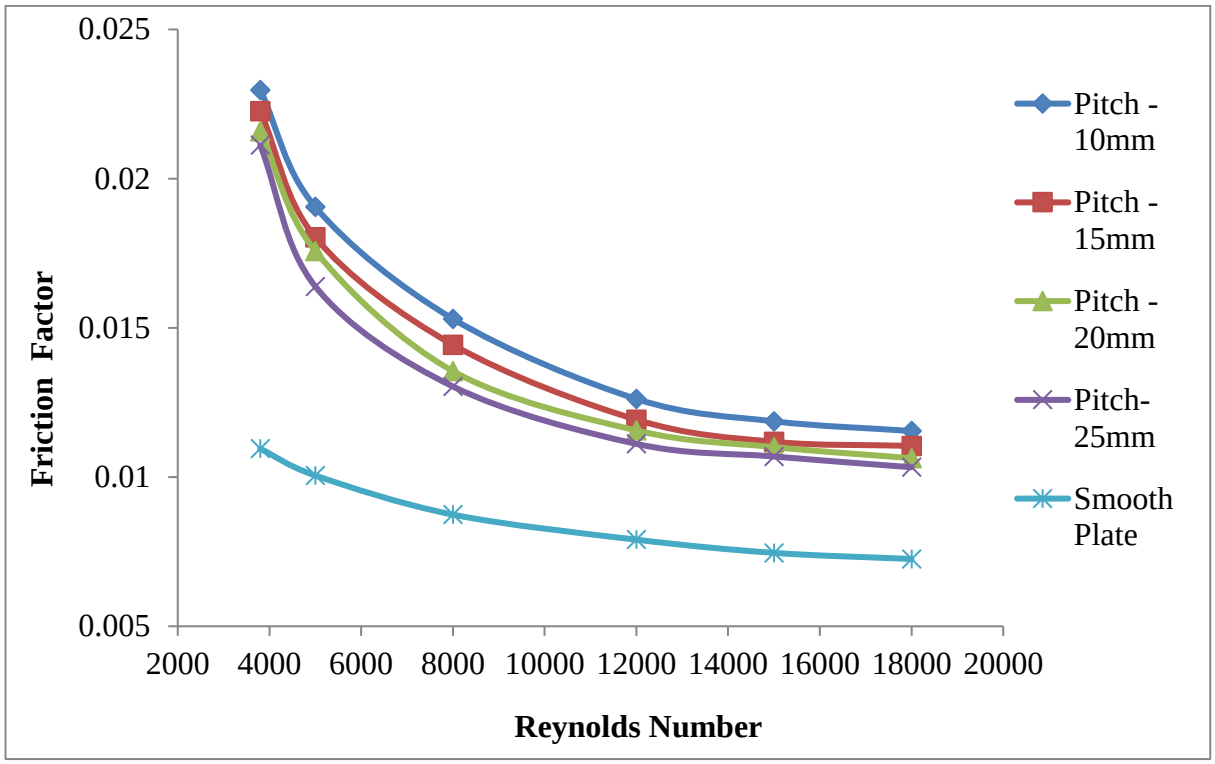

Fig. 4.21 Friction factor against Reynolds Number at design-2

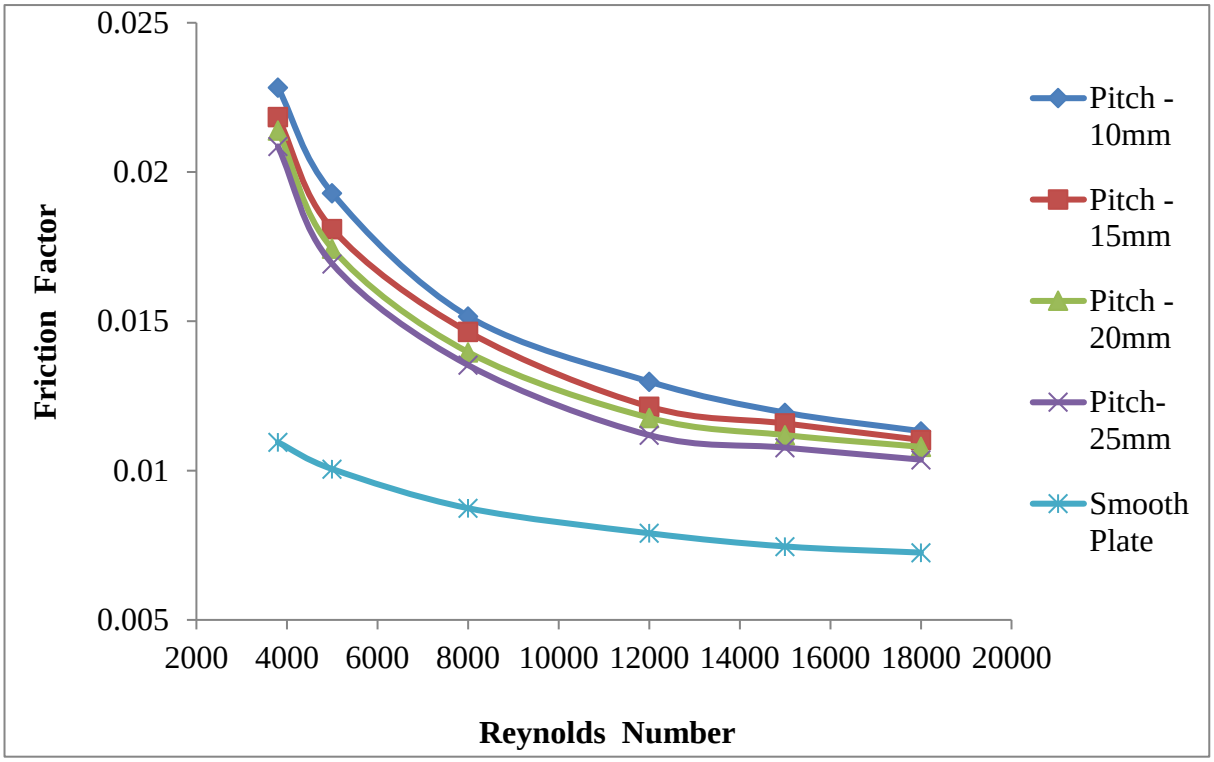

Fig. 4.22 Friction factor against Reynolds Number at design-3

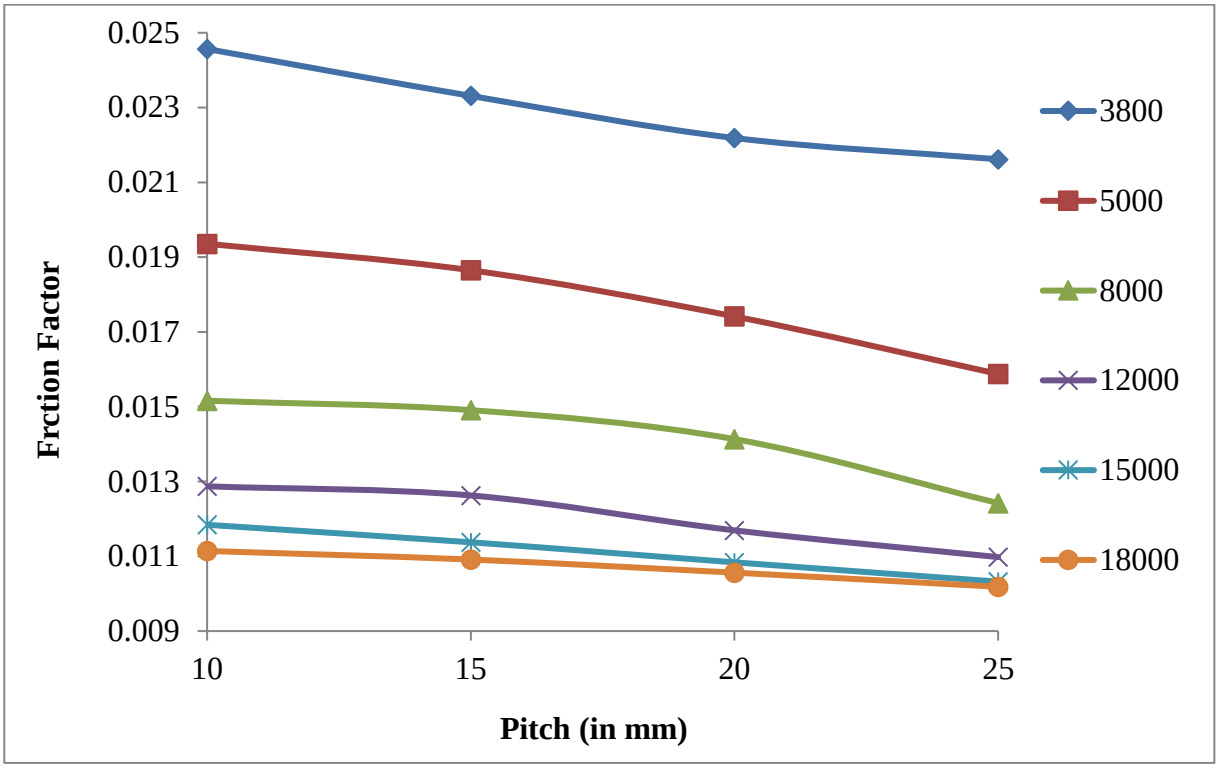

Fig. 4.23 Variation of Friction factor against pitch at design-1

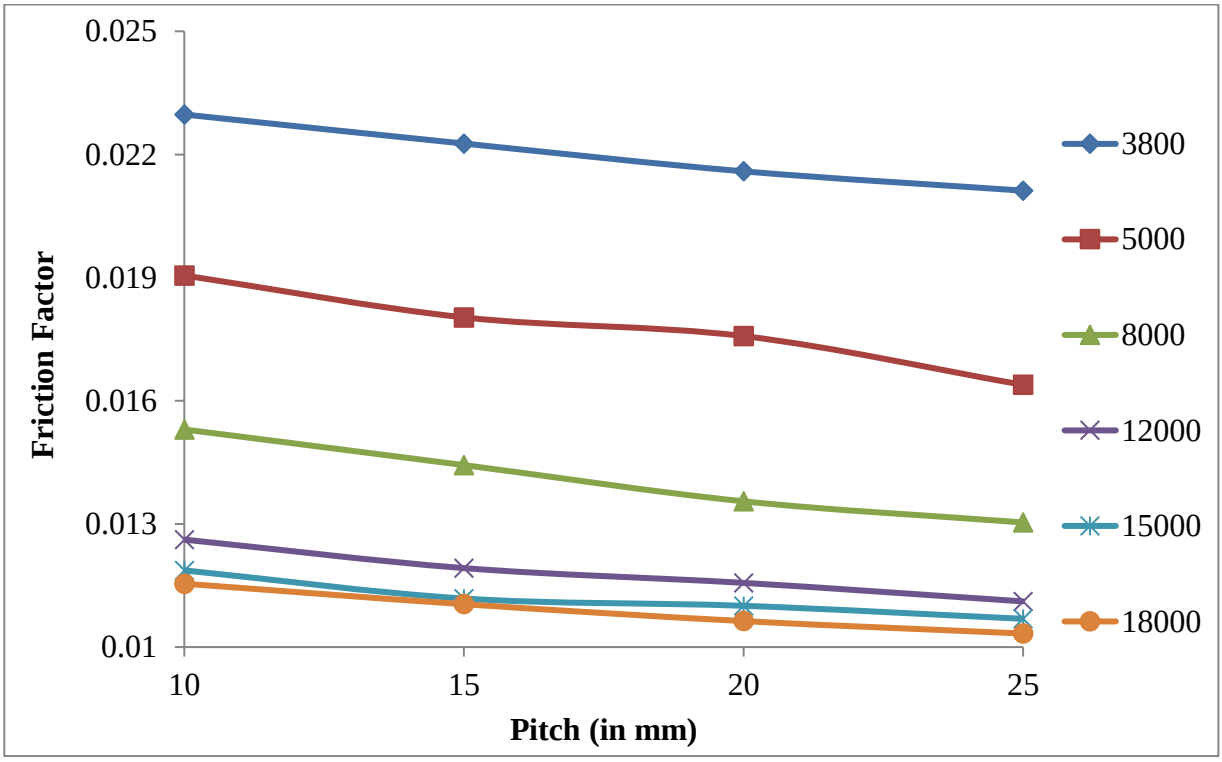

Fig. 4.24 Variation of Friction factor against pitch at design-2

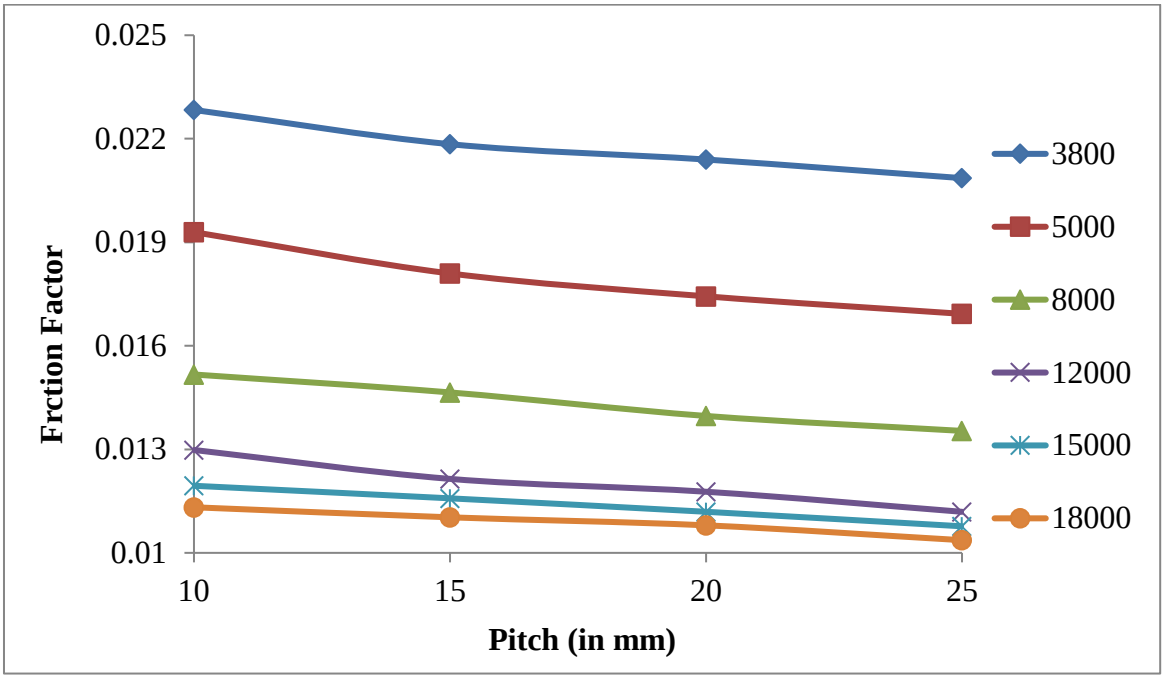

Fig. 4.25 Variation of Friction factor against pitch at design-3

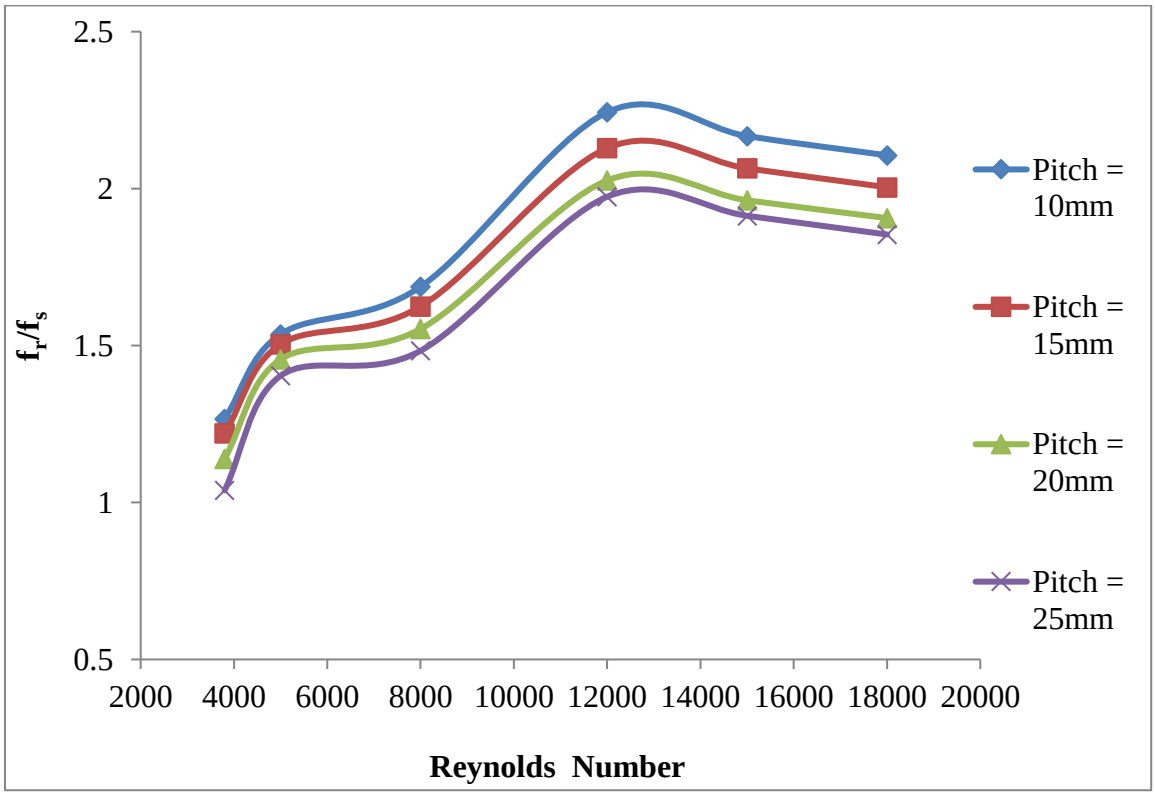

Fig. 4.26 Enhancement ratio of Friction factor against Reynolds Number at design- 1

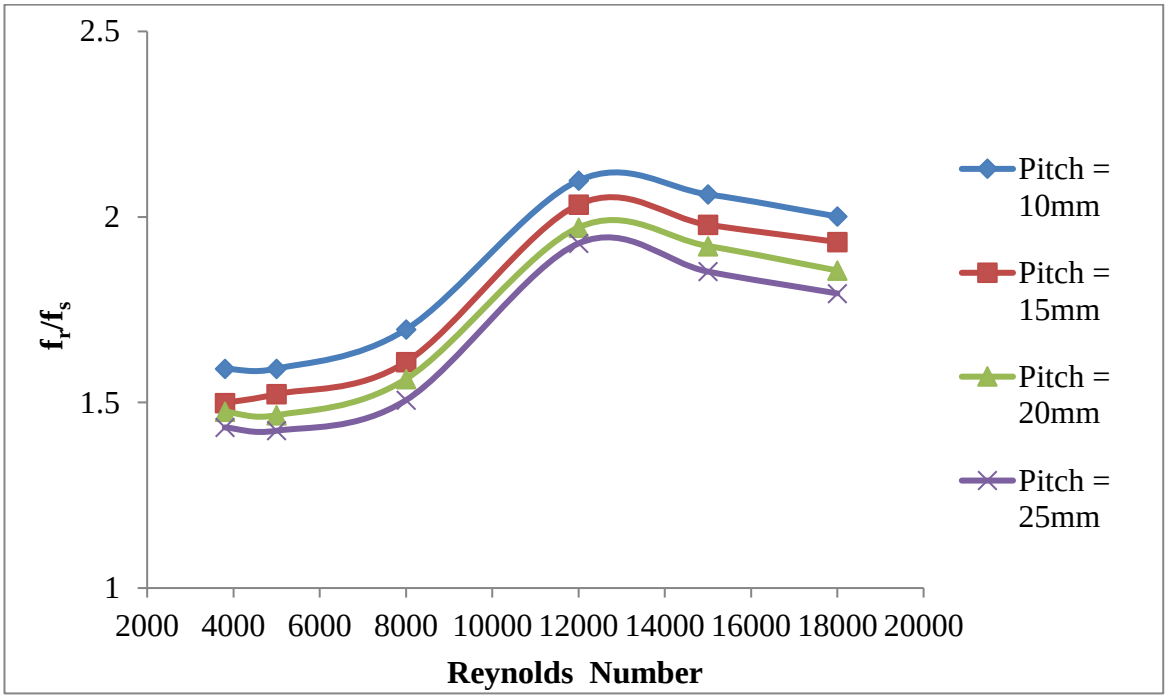

Fig. 4.27 enhancement ratio of Friction factor against Reynolds Number at design- 2

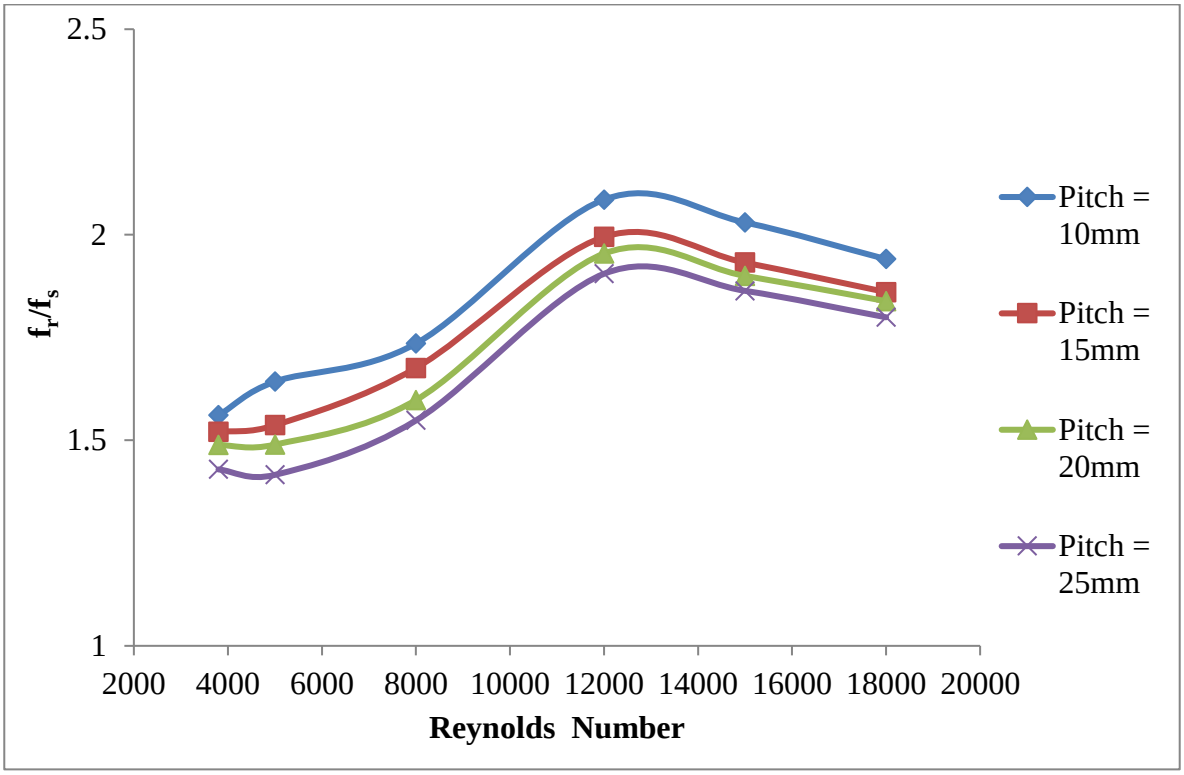

Fig. 4.28 Enhancement ratio of Friction factor against Reynolds Number at design- 3

Figs. 4.26, 4.27, and **4.28** show the enhancement ratio of friction factor for obtuse L- roughness relative to the smooth surface for various roughness configurations. The fact

that values of friction factor are more than unity indicates that there is more friction present during fluid flow than there would be on a smooth surface. This phenomenon is obvious in roughness geometries because roughness geometries provide more friction losses than smooth surfaces. The statistics also demonstrate that the enhancement ratio of the friction factor rises as the Reynolds number rises. This shows that frictional losses rise at higher Reynolds numbers in comparison to a smooth surface.

4.7 Effect on the Thermo-Hydraulic Performance Parameter

The thermal performance of a solar air heater is considerably improved by artificial roughness. The heat transfer coefficient rises when turbulence close to the absorber surface increases. The Nusselt number rises as a result of the convective heat transfer coefficient increasing due to greater turbulence. However, the pumping loss also increases as turbulence levels increases. Thus, improved thermal performance is at the expense of improved hydraulic performance. As a result, the performance parameter is determined taking into account both thermal and hydraulic components of the solar air heater in order to determine the optimal thermo-hydraulic performance. Thermo-hydraulic performance parameter (THPP) vs. Reynolds number for all 3 designs of absorber plate roughness is shown in **Fig. 4.29, 4.30,** and, **4.31**.

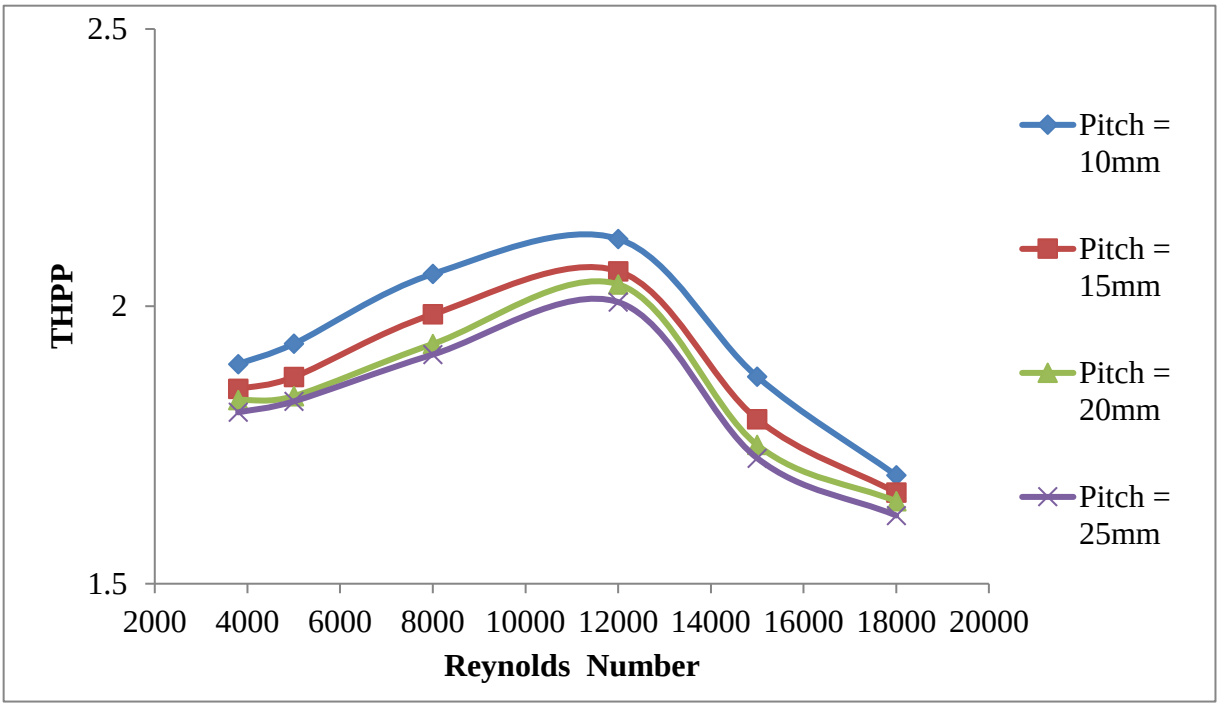

Fig. 4.29 THPP against Reynolds Number at design- 1

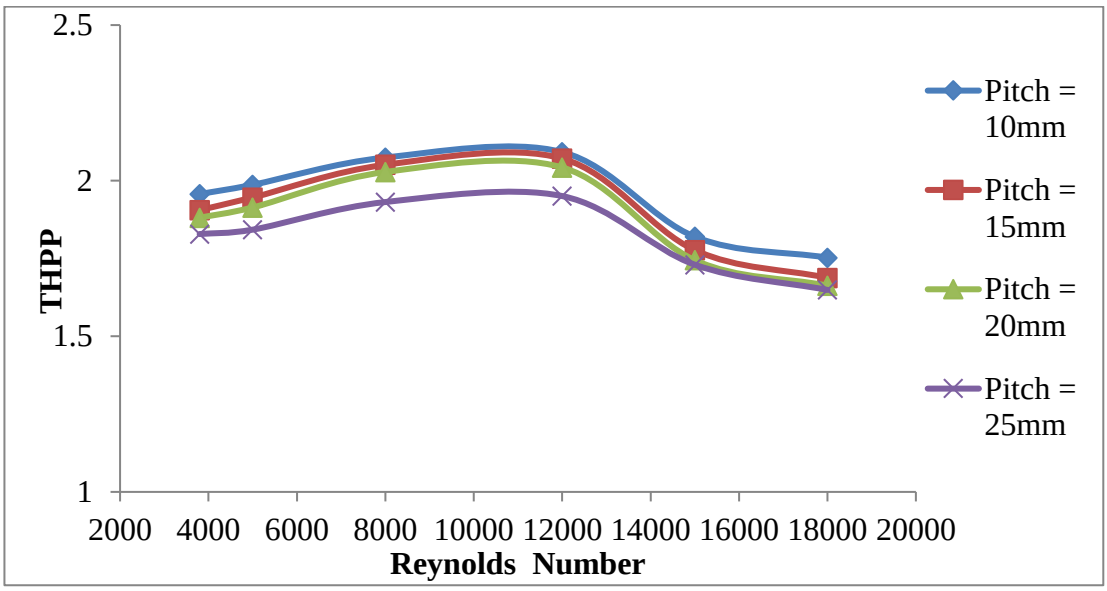

Fig. 4.30 THPP against Reynolds Number at design- 2

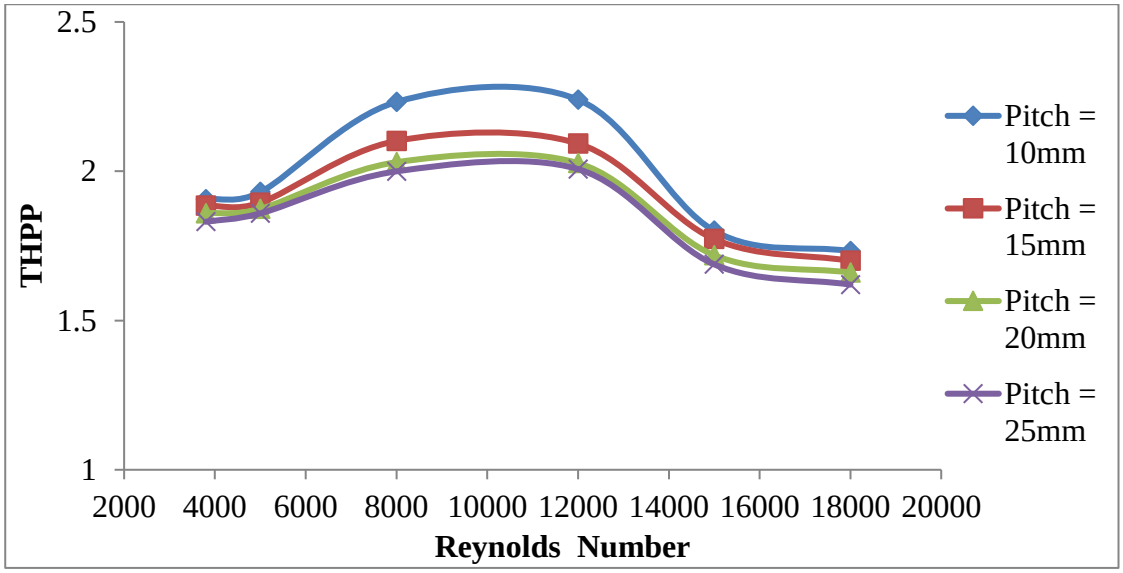

Fig. 4.31 THPP against Reynolds Number at design- 3

The patterns reveal that the Thermo-hydraulic performance parameter (THPP) increases to a maximum value and then decreases with the continuous increment of the Reynolds number. It is also clear that maximum THPP for different geometries is often reached around the Reynolds number value of 12,000. The disturbances brought by the artificial roughness can be used to explain the phenomenon. Initially, due to the lower Reynolds number and lower velocity, the transfer of heat is not much effective and the friction factor is also higher. As the Reynolds number increases, it increases the local disturbance near to the collector plate and which is able to transfer more heat and got a

higher Thermo-hydraulic performance parameter (THPP). When the Reynolds number is raised even further, it increases the turbulence which improves the heat transmission, but the pressure drop also rises more quickly, which reduces the value of the Thermo-hydraulic performance parameter (THPP). In the current study, the Reynolds number of 12000 corresponds to the maximum value of the Thermo-hydraulic performance parameter (THPP).

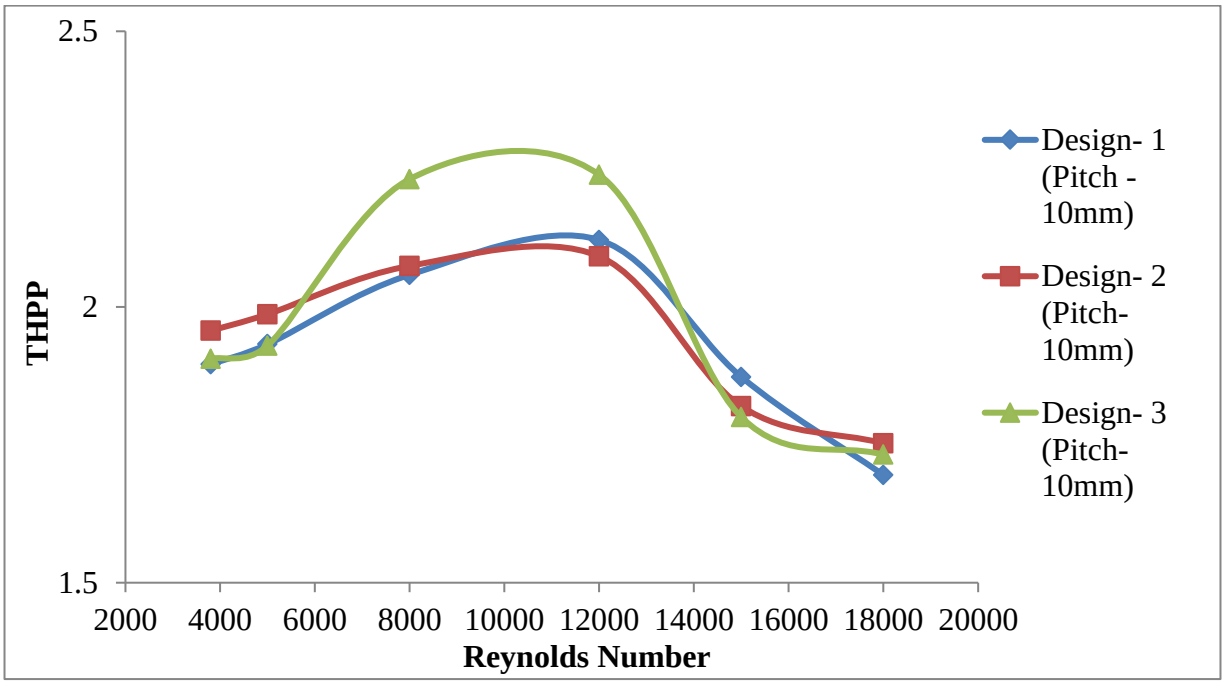

Fig. 4.32 Maximum THPP against Reynolds Number in all design combinations

From **Fig 4.32**, it can be seen that design- 3, having a pitch of 10 mm is showing the highest value of the Thermo- hydraulic performance parameter (THPP). The results show that design- 3 with a pitch of 10 mm and Reynolds number of 12,000 produces the highest value of THPP. In the set of parameters examined within this work, the maximum THPP value is found to be 2.239.

Closer

In this chapter, results obtained from numerical solution are compared with previous work as well as analytical solution which including variation on Nusselt number and variation on friction factor. Nusselt number, Friction factor and Thermo- Hydraulic Performance Parameter (THPP) for different geometry and operating parameter are compared and discussed.

Summary and Conclusions

Chapter 5 SUMMARY AND CONCLUSIONS

5.1 General

In the current work, a two-dimensional numerical study of a solar air heater with artificially created obtuse- L roughness was carried out. CFD outcomes for thermal as well as hydraulic behavior for various artificial roughness configurations were compared with the conventional smooth flat plate solar air heater.

The key findings from the investigations are summarized in the following paragraphs:

1. To get information on solar air heaters, a CFD model that includes an artificial obtuse- L roughness was created, verified, and used.
2. Nusselt number and friction factor findings are validated with standard equations and results of Yadav and Bhagoria (2014) for a smooth absorber plate.
3. For assuring the reliability of the current model, validation has been conducted as per Yadav and Bhagoria's (2014) results for the geometry they employed.
4. Results from empirical relations for Nusselt number and friction factor were found to differ from CFD results by an order of 9.07% and 2.95%, respectively.
5. Results of Yadav and Bhagoria (2014) for Nusselt number and friction factor were found to differ from CFD results by an order of 4.92% and 3.93%, respectively for a rectangular roughness which has rib height and pitch are an order of 1.4 mm and 10 mm.
6. For getting the best Obtuse-L angle, I have taken 7 different angles as 90^o, 105^o, 120^o, 135^o, 150^o, 165^o, and 180^o in the interval of 15^o. After calculating the results, it can be seen that the 165^o angle has the highest Nusselt number value of around 93.20 at the 12000 Reynolds number. So, the further calculation has been done on 165^o.
7. I have taken 3 designs based on the design of obtuse-L. Design-1 has obtuse-L roughness, design-2 has opposite obtuse-L roughness, and design- 3 has a combination of both of them. A total of 4 pitch 10 mm, 15 mm, 20 mm, and 25 mm have been taken into consideration.

8. With an increase in Reynolds number, the Nusselt number enhancement ratio increases more quickly, and subsequently, after reaching a certain value of Reynolds Number, the enhancement ratio almost stops rising.
9. The Friction Factor Enhancement Ratio rises rapidly as Reynolds Number rises; hence, once Reynolds Number reaches a specific value, the enhancement ratio almost stops increasing.
10. As the Reynolds number rises, the friction factor decreases for all pitch values.
11. The Thermo-hydraulic performance parameter (THPP) patterns increase to the maximum value and then decrease with the continuous increment of the Reynolds number.
12. The maximum Thermo-hydraulic Performance parameter (THPP) for all geometries is typically reached around the Reynolds number value of 12000. The maximum THPP value is found to be 2.239 in design-3 of pitch 10 mm.

5.2 Future scope

According to the results of this paper, there is plenty of scope for further research on artificially roughened solar air heaters with various roughness geometries, including:

1. Several aerofoil profiles.
2. Combination of L-shaped and V-shaped rib profiles.
3. Obtuse- L roughness profile on double pass solar air heater.

Literature Cited

LITERATURE CITED

Aharwal, K. R., Gandhi, B. K. and Saini, J. S. 2009. Heat transfer and friction characteristics of solar air heater ducts having integral inclined discrete ribs on absorber plate. *Int. J. Heat Mass Transf.,* 52 (25): 5970-5977.

Alam, T., Saini, R. P. and Saini, J. S. 2014. Use of tubulators for heat transfer augmentation in an air duct-a review. *J. Renew. Energy*, 62:689-715.

Alam, T., Saini, R. P. and Saini, J. S. 2014. Heat and flow characteristics of air heater ducts provided with turbulators. *J. Renew. Sustain. Energy Rev.,* 31:289-304.

Bhagoria, J. L., Saini, J. S. and Solanki, S. C. 2002. Heat transfer coefficient and friction factor correlations for rectangular solar air heater duct having transverse wedge shaped rib roughness on the absorber plate. *J. Renew. Energy,* 25 (3): 341-369.

Bopche, S. B. and Tandale, M. S. 2009. Experimental investigations on heat transfer and frictional characteristics of a turbulator roughened solar air heater duct**.** *Int. J. Heat Mass Transf.,* 52 (11-12): 2834-2848.

Chamoli, S., Chauhan, R., Thakur, N. S. and Saini, J. S. 2012. A review of the performance of double pass solar air heater. *J. Renew. Sustain. Energy Re*v., 16: 481-492.

Chaube, A., Sahoo, P. K. and Solanki, S. C. 2006. Analysis of heat transfer augmentation and flow characteristics due to rib roughness over absorber plate of a solar air heater. *J. Renew. Energy,* 31 (3): 317-331.

Gabhane, M. G. and Patil, A. B. K. 2017. Experimental analysis of double flow solar air heater with multiple C shape roughness. *J. Sol. Energy*, 155:1411-1416.

Gupta, D., Solanki, S. C. and Saini, J. S. 1993. Heat and fluid flow in rectangular solar air heater ducts having transverse rib roughness on absorber plates. *J. Sol. Energy*, 51: 31-37.

Gupta, D., Solanki, S. C. and Saini, J. S. 1997. Thermo-hydraulic performance of solar air heaters with roughened absorber plates. *J. Sol. Energy*, 61(1): 33-42.

Gupta, M. K. and Kaushik, S. C. 2009. Performance evaluation of solar air heater having expanded metal mesh as artificial roughness on absorber plate. *Int. J. Therm. Sci*., 48: 1007-1016.

Haldar, A., Varshney, L. and Verma, P. 2022. Effect of roughness parameters on the performance of solar air heater having artificial wavy roughness using CFD. *J. Renew. Energy*, 184: 266-279.

Hans, V. S., Saini, R. P. and Saini, J. S. 2009. Performance of artificially roughened solar air heaters a review. *J. Renew. Sustain. Energy Rev.*, 13 (8): 1854-1869.

Hans, V. S., Saini, R. P. and Saini, J. S. 2010. Heat transfer and friction factor correlations for a solar air heater duct roughened artificially with multiple v-ribs. *J. Sol. Energy*, 84 (6): 898-991.

Jaurker, A. R., Saini, J. S. and Gandhi, B. K. 2006. Heat transfer and friction characteristics of rectangular solar air heater duct using rib-grooved artificial roughness. *J. Sol. Energy*, 80 (8): 895-907.

Joule. 1861. Philosophical Transactions. The Royal Society of London, London. 834p.

Kalpana, Varshney, L., and Subudhi, S. 2022. Heat Transfer and Pressure Drop in a Double-Pass Solar Air Heater with Arc-Shaped Artificial Roughness. *J. Sol. Energy Eng*., 144(6): 061002.

Karmare, S. V. and Tikekar, A. N. 2007. Heat transfer and friction factor correlation for artificially roughened duct with metal grit ribs. *Int. J. Heat Mass Transf.*, 50: 4342-4351.

Karmare, S. V. and Tikekar, A. N. 2010. Experimental investigation of optimum thermohydraulic performance of solar air heaters with metal rib grits roughness. *J. Sol. Energy*, 83 (1): 6-13.

Karwa, R. and Shrivastava, P. 2013. Experimental studies of augmented heat transfer and friction in asymmetrically heated rectangular ducts with ribs on heated wall in transverse inclined, v-continuous and v-discrete pattern. *Int. J. Commun. Heat Mass Transf.*, 30 (2): 241-250.

Karwa, R., Solanki, S. C. and Saini, J. S. 2001. Thermo-hydraulic performance of solar air heaters having integral chamfered rib roughness on absorber plates. *J. Energy*, 26 (2): 161-176.

Komolafe, C. A., Oluwaleye, I. O., Awogbemi, O. and Osueke, C. O. 2019. Experimental investigation and thermal analysis of solar air heater having rectangular rib roughness on the plate. *Case Stud. Therm. Eng.*, 14:100442.

Kumar, A., Bhagoria, J. L. and Sarviya, R. M. 2009. Heat transfer and friction correlations for artificially roughened solar air heater duct with discrete w-shaped ribs. *J. Energy Convers. Manag.,* 50 (8): 2106-2117.

Kumar, A. and Layek, A. 2019. Energetic and exergetic performance evaluation of solar air heater with twisted rib roughness on absorber plate. *J. Clean. Prod.*, 232: 617-628.

Kumar, A., Saini, R. P. and Saini, J. S. 2012. Heat and fluid flow characteristics of roughened solar air heater ducts. *J. Renew. Energy*, 47: 77-94.

Kumar, A., Saini, R. P. and Saini, J. S. 2012. Experimental investigation on heat transfer and fluid flow characteristics of air flow in a rectangular duct with multi v shaped rib with gap roughness on the heated plate. *J. Sol. Energy*, 86 (6): 1733-1749.

Kumar, R., Goel, V., Singh, P., Saxena, A., Kashyap, A. and Rai, A. 2019. Performance evaluation and optimization of solar-assisted air heater with discrete multiple arc-shaped ribs. *J. Energy Storage*, 26:100978.

Kumar, S. and Saini, R. P. 2009. CFD based performance analysis of a solar air heater duct provided with artificial roughness. *J. Renew. Energy*, 34 (5): 1285-1291.

Lanjewar, A., Bhagoria, J. L. and Surviya, R. M. 2011. Heat transfer and friction in solar air heater duct with w-shaped rib roughness on absorber plate. *J. Renew. Energy*, 36 (7): 4531-4541.

Layek, A., Saini, J. S. and Solanki, S. C. 2007. Second law optimization of a solar air heater having chamfered rib-groove roughness on absorber plate. *J. Renew. Energy*, 32: 1967-1980.

Layek, A., Saini, J. S. and Solanki, S. C. 2007. Heat transfer and friction characteristics for artificially roughened ducts with compound turbulators. *Int. J. Heat Mass Transf.*, 50 (23-24): 4845-4854.

Lewis, D. K. 1975. Minnesota Studies in the Philosophy of Science. University of Minnesota Press, Minnesota. 35p.

Mahanand, Y. and Senapati, J. 2020. Thermal enhancement study of a transverse inverted T-shaped ribbed solar air heater. *Int. J. Commun. Heat Mass Transf.*, 119:104922.

Mittal, M. K. and Varshney, L. 2006. Optimum Thermohydraulic performance of a wire mash packed Solar air heater. *J. Sol. Energy*, 80: 1112-1120.

Mittal, M. K., Varun, Saini, R. P. and Singal, S. K. 2007. Effective efficiency of solar air heaters having different types of roughness elements on the absorber plate. *J. Energy*, 32:739-745.

Momin, A. M. E., Saini, J. S. and Solanki, S. C. 2002. Heat Transfer and Friction in Solar Air Heater Duct with V-Shaped Rib Roughness on Absorber Plate. *Int. J. Heat Mass Transf.*, 45 (16): 3383-3396.

Patil, A. K., Saini, J. S., and Kumar, K. 2012. A comprehensive review on roughness geometries and investigation techniques used in artificially roughened solar air heaters. *Int. J. Heat Mass Transf.*, 2(1): 1-15.

Patankar, S. V. 1980. Numerical heat transfer and fluid flow. Hemisphere Publishing Corporation, New York. 244p.

Prasad, B. N. 2013. Thermal performance of artificially roughened solar air heaters. *J. Sol. Energy*, 91: 59-67.

Prasad, B. N. and Saini, J. S. 1988. Effect of artificial roughness on heat transfer and friction factor in a solar air heater. *J. Sol. Energy*, 41(6): 555-560.

Rai, G. D. 2010. Non conventional Energy Recourses. Khanna Publishers, New Delhi. 912p.

Ravi, R. K. and Saini, R. P. 2016. A review on different techniques used for performance enhancement of double pass solar air heaters. *J. Renew. Sustain. Energy Rev.*, 56: 941-952.

Pramanik, R. N., Sahoo, S. S., Swain, R. K., Mohapatra, T. P. and Srivastava, A. K. 2017. Performance analysis of double pass solar air heater with bottom extended surface. *J. Energy procedia*. 109: 331-337.

Sahu, M. M. and Bhagoria, J. L. 2005. Augmentation of heat transfer coefficient by using 90° broken transverse ribs on absorber plate of solar air heater. *J. Renew. Energy*, 30 (13): 2057-2073.

Saini, R. P. and Verma, J. 2008. Heat transfer and friction factor correlations for a duct having dimple-shaped artificial roughness for solar air heaters. *J. Energy*, 33 (8): 1277-1287.

Saini, R. P. and Saini, J. S. 1997. Heat transfer and friction factor correlations for artificially roughened ducts with expanded metal mesh as roughened element. *Int. J. Heat Mass Transf.*, 40 (4): 973-986.

Saini, S. K. and Saini, R. P. 2008. Development of correlations for nusselt number and friction factor for solar air heater with roughened duct having arc-shaped wire as artificial roughness. *J. Sol. Energy*, 82 (12): 1118-1130.

Sayigh, A. A. M. 1979. Solar Energy Engineering. Academic Press, Londan. 526p.

Sethi, M., Varun and Thakur, N. S. 2012. Correlations for solar air heater duct with dimpled shape roughness elements on absorber plate. *J. Sol. Energy*, 86 (9): 2852-2861.

Sharma, A. K. and Thakur, N. S. 2012. CFD based fluid flow and heat transfer analysis of a v-shaped roughened surface solar air heater. *Eng. Sci. Technol. an Int. J.*, 4 (5): 2115-2121.

Singh, S., Chander, S. and Saini, J. S. 2011. Heat transfer and friction factor correlations of solar air heater ducts artificially roughened with discrete v-down ribs. *J. Energy*, 36 (8): 5053-5064.

Singh, S. Chander, S. and Saini, J. S. 2012. Exergy based analysis of solar air heater having discrete V-down rib roughness on absorber plate. *J. Energy*, 37 (1): 749-758.

Sukhatme, S. and Nayak, J. 2011. Solar Energy principles of Thermal Collection and Storage. Tata McGraw Hill, New York. 354p.

Tyagi, V. V., Panwar, N. L., Rahim, N. A. and Kothari, R. 2012. Review on solar air heating system with and without thermal energy storage system. *J. Renew. Sustain. Energy Rev.,* 16 (4): 2289-2303.

Varshney, L. and Saini, J. S. 1998. Heat transfer and friction factor correlations for rectangular solar air heater duct packed with wire mesh screen matrices. *J. Sol. Energy*, 62: 255-262.

Varun, Saini, R. P. and Singal, S. K. 2008. Investigation of thermal performance of solar air heater having roughness elements as a combination of inclined and transverse ribs on the absorber plate. *J. Renew. Energy*, 33(6): 1398-1405.

Varun, Saini, R. P. and Singal, S. K. 2007. A review on roughness geometry used in solar air heaters. *J. Sol Energy*, 81(11): 340-350.

Verma, S. K. and Prasad, B. N. 2000. Investigation for the optimal thermos-hydraulic performance of artificially roughened solar air heaters. *J. Renew. Energy,* 20(1): 19-36.

Yadav, A. S. and Bhagoria, J. L. 2013. Renewable energy sources an application guide. *Int. J. Energy Res.,* 3 (2): 70-90.

Yadav, A. S. and Bhagoria, J. L. 2013. A CFD analysis of a solar air heater having triangular rib roughness on the absorber plate.*Int. J. Chemtech Res.,* 5(2): 964-971.

Yadav, A. S. and Bhagoria, J. L. 2013. A CFD based heat transfer and fluid flow analysis of a solar air heater provided with circular transverse wire rib roughness on the absorber plate. *J. Energy*, 55: 1127-1142.

Yadav, A. S. and Bhagoria, J. L. 2013. A CFD based heat transfer and fluid flow analysis of a conventional solar air heater. *J. Eng. Educ.*, 6(2): 138-147.

Yadav, A. S. and Bhagoria, J. L. 2014. A numerical investigation of turbulent flows through an artificially roughened solar air heater. *J. Numer. Heat Transf.*, 165(7):679-698.

CURRICULUM VITAÉ

Name: Rahul Pant

Phone Number: 7535940141

Mailing Address:
Rahul Pant
Village- Jeolikote, P.O.- Jeolikote,
District- Nainital,
Uttarakhand (263127)
rahulpant950@gmail.com

Permanent Address:
Village- Jeolikote,
P.O. – Jeolikote,
District- Nainital,
Uttarakhand (263127)

Career Objective: To work in field of Simulation analysis.

Educational Qualification:

S. No.	Examination passed	Institution	Year	Percentage/ CGPA
1.	M.Tech.	Govind Ballabh Pant University of Agriculture &Technology, Pantnagar, Uttarakhand	2022	Pursuing
2.	B. Tech.	Graphic Era Hill University, Bhimtal campus, Uttarakhand	2019	79.50
3.	Intermediate	Government Inter College, Jeolikote	2015	70.60
4.	High School	Government Inter College, Jeolikote	2013	65.20

- **Specialization:** Major: Thermal Engineering
- **Thesis Title: CFD Simulation of Solar air heater using Obtuse L roughness**
- **Conferences/Seminars/Workshops/Training Attended:** ANSYS and HyperWorks Basic to professional Training program from Ardent, Pune. ANSYS Training program from Ardent Computech Private Limited Kolkata, ANSYS workshop by ARK solution Private Limited, Pune.
- **Software skills:** ANSYS, HyperWorks, Python, SolidWorks, MS-Office, AutoCAD
- **Professional skill:** Computational Fluid Dynamics

Place: Pantnagar
Date: September, 2022

(Rahul Pant)

Name	: Rahul Pant	**Id. No.**	: 57092
Semester & year of admission	: 1st Semester, 2020-2021	**Degree**	: M. Tech (Mechanical Engineering)
Major	: Thermal Engineering	**Department**	: Mechanical Engineering
Thesis Title	:**CFD Simulation of Solar air heater using Obtuse L roughness**		
No. of pages	: 59	**Advisor**	: Dr. Lokesh Varshney

ABSTRACT

In the present work, Computational Fluid Dynamics (CFD) analysis of solar air heater having Obtuse L roughness has been performed. ANSYS FLUENT software is used as a simulation tool for CFD analysis. Twelve different configurations of Roughened surface having roughness angle of 165^{o} and have pitch of 10, 15, 20 and 25 have been considered. A two-dimensional computational domain is modelled and the involved differential equations are solved using a finite volume method. The RNG k-ε turbulence model with enhanced wall function is used to solve the transport equations for turbulent flow and energy dissipation rate. Effect of roughness parameter on Nusselt number, friction factor, and thermo-hydraulic performance parameter are studied for uniform heat flux of 1000 W/m^2. The optimal values of geometric parameters are obtained on the basis of the thermo-hydraulic performance parameter in the range of the Reynolds number from 3800 to 18000. Optimum thermo-hydraulic performance parameter is found to be 2.23 corresponding to the Design- 3 having pitch of 10 mm at Reynolds number of 12000.

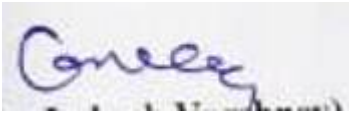

(Dr. Lokesh Varshney)
Advisor

(Rahul Pant)
Author

नाम	: राहुल पंत	परिचायंक	: ५७०९२
सत्र , प्रवेशवर्ष	: प्रथम ,२०२०-२०२१	डिग्री	: स्नातकोत्तर
मेजर	: उष्ण अभियांत्रिकी	विभाग	: यान्त्रिक अभियांत्रिकी
शोधशीर्षक	: **ओबट्यूज एल खुरदरापन का उपयोग कर सोलर एयर हीटर का सीएफडी सिमुलेशन**		
पृष्ठों की संख्या	: ५९	सलाहकार	: डॉ. लोकेश वार्ष्णेय

सारांश

वर्तमान कार्य में, अधिक L खुरदरापन वाले सोलर एयर हीटर का कम्प्यूटेशनल फ्लूड डायनेमिक्स (सीएफडी) विश्लेषण किया गया है। ANSYS FLUENT सॉफ़्टवेयर का उपयोग सीएफडी विश्लेषण के लिए सिमुलेशन टूल के रूप में किया जाता है। १६५° के खुरदरेपन वाले कोण और १०, १५, २० और २५ मिमी की पिच वाली खुरदरी सतह के बारह अलग-अलग विन्यासों पर विचार किया गया है। एक द्वि-आयामी कम्प्यूटेशनल डोमेन का मॉडल तैयार किया जाता है और इसमें शामिल अंतर समीकरणों को एक परिमित मात्रा पद्धति का उपयोग करके हल किया जाता है। बढ़ी हुई दीवार फ़ंक्शन के साथ आरएनजी के-ε अशांति मॉडल का उपयोग अशांत प्रवाह और ऊर्जा अपव्यय दर के लिए परिवहन समीकरणों को हल करने के लिए किया जाता है। नसेल्ट संख्या, घर्षण कारक, और थर्मो-हाइड्रोलिक प्रदर्शन पैरामीटर पर खुरदरापन पैरामीटर के प्रभाव का अध्ययन १००० W/m^2 के समान ताप प्रवाह के लिए किया जाता है। ३८०० से १८००० तक रेनॉल्ड्स संख्या की सीमा में थर्मो-हाइड्रोलिक प्रदर्शन पैरामीटर के आधार पर ज्यामितीय मापदंडों का इष्टतम मान प्राप्त किया जाता है। इष्टतम थर्मो-हाइड्रोलिक प्रदर्शन पैरामीटर डिजाइन - ३ के अनुरूप २.२३ पाया गया है जिसमें १० मिमी की पिच है और रेनॉल्ड्स संख्या १२००० है।

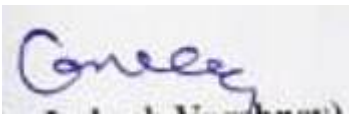

(डॉ. लोकेश वार्ष्णेय)
सलाहकार

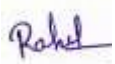

(राहुल पंत)
लेखक